TITLE:

Mechanistic insights into intramembrane proteolysis by E. coli site-2 protease homolog RseP

AUTHOR(S):

Imaizumi, Yuki; Takanuki, Kazunori; Miyake, Takuya; Takemoto, Mizuki; Hirata, Kunio; Hirose, Mika; Oi, Rika; ... Hizukuri, Yohei; Akiyama, Yoshinori; Nogi, Terukazu

京都大学学術情報リポジトリ

KURENAI 紅

Kyoto University Research Information Repository

SCIENCE ADVANCES | RESEARCH ARTICLE

STRUCTURAL BIOLOGY

Mechanistic insights into intramembrane proteolysis by *E. coli* site-2 protease homolog RseP

Yuki Imaizumi[1]†, Kazunori Takanuki[1]†, Takuya Miyake[2]†, Mizuki Takemoto[3], Kunio Hirata[4], Mika Hirose[5], Rika Oi[1], Tatsuya Kobayashi[2], Kenichi Miyoshi[2], Rie Aruga[1], Tatsuhiko Yokoyama[2], Shizuka Katagiri[1], Hiroaki Matsuura[4], Kenji Iwasaki[6], Takayuki Kato[5], Mika K. Kaneko[7], Yukinari Kato[7,8], Michiko Tajiri[1], Satoko Akashi[1], Osamu Nureki[3], Yohei Hizukuri[2]*, Yoshinori Akiyama[2]*, Terukazu Nogi[1]*

Site-2 proteases are a conserved family of intramembrane proteases that cleave transmembrane substrates to regulate signal transduction and maintain proteostasis. Here, we elucidated crystal structures of inhibitor-bound forms of bacterial site-2 proteases including *Escherichia coli* RseP. Structure-based chemical modification and cross-linking experiments indicated that the RseP domains surrounding the active center undergo conformational changes to expose the substrate-binding site, suggesting that RseP has a gating mechanism to regulate substrate entry. Furthermore, mutational analysis suggests that a conserved electrostatic linkage between the transmembrane and peripheral membrane-associated domains mediates the conformational changes. In vivo cleavage assays also support that the substrate transmembrane helix is unwound by strand addition to the intramembrane β sheet of RseP and is clamped by a conserved asparagine residue at the active center for efficient cleavage. This mechanism underlying the substrate binding, i.e., unwinding and clamping, appears common across distinct families of intramembrane proteases that cleave transmembrane segments.

INTRODUCTION

Intramembrane proteolysis—hydrolysis of a peptide bond within the lipid bilayer—is implicated in a variety of cellular processes throughout all three domains of life, including signal transduction and membrane protein homeostasis (*1–3*). In humans, deregulation of this cleavage leads to diseases such as Alzheimer's disease (*4*, *5*), while signal transduction through intramembrane proteolysis is associated with pathogenic infections (*6*, *7*). The substrate cleavage is catalyzed by four distinct families of intramembrane proteases, each classified on the basis of catalytic mechanism: the zinc metalloprotease site-2 protease (S2P), the aspartic protease presenilin/signal peptide peptidase (SPP), the serine protease Rhomboid, and the glutamic protease Ras-converting enzyme 1 (Rce1) (*8*, *9*), among which S2P, presenilin/SPP, and Rhomboid cleave transmembrane (TM) segments of substrates. Eukaryotic S2Ps, including human S2P, have been identified in signal transduction for lipid metabolism (*10–12*) and endoplasmic reticulum stress responses (*13*), in which they perform the intramembrane proteolysis of transcription factor precursors after the extracytoplasmic cleavage of the substrates by site-1 protease (S1P). RseP from *Escherichia coli* is an S2P homolog classified in the same subfamily

(group I) as human S2P (Fig. 1, A and B) (*1*, *14*, *15*). RseP is also involved in the second step of sequential cleavage of type II membrane proteins for signal transduction. RseP cleaves the TM segment of anti–sigma factor RseA in the extracytoplasmic stress response after the periplasmic region of RseA is cleaved off by the membrane-anchored protease DegS (Fig. 1D) (*16–18*). In RseP, two tandemly arranged periplasmic PDZ domains (PDZ tandem) were proposed to serve as a size exclusion filter to sterically hinder active site entry by any substrate having a bulky periplasmic domain (*19–21*). This substrate discrimination by size exclusion was also proposed for the human S2P, which has an extracytoplasmic PDZ domain (*22*). Besides, S2Ps are presumed to have a β sheet in the proximity of the active center in the TM domain commonly (*23*, *24*). RseP is also predicted to have two intramembrane β hairpins (fig. S1), which were shown to bind the substrate near the bond that is cleaved and to contribute to substrate discrimination (*24*, *25*). However, the absence of structural data hampers understanding of how site-1–cleaved substrates pass through the size exclusion filter to access the active center and of how the substrate TM segments exactly bind with the intramembrane β sheet of S2Ps. Because the active center of S2Ps is predicted to be located within the hydrophobic milieu of the lipid bilayer, it must both form a hydrophilic compartment around the catalytic zinc for efficient hydrolysis and accommodate hydrophobic segments of the substrate TM domain. Concerning the S2P family, a crystal structure including the active center is available for the TM domain of the archaeon *Methanocaldococcus jannaschii* S2P homolog (*Mj*S2P) (*26*). However, *Mj*S2P belongs to the group III subfamily of S2P and does not have PDZ domains in the extracytoplasmic region (Fig. 1C) (*15*). Furthermore, *Mj*S2P was proposed to regulate substrate entry by using the TM helices flanking the catalytic core TM domain as a gate, but those helices are not present in group I S2Ps such as *Ec*RseP and human S2P. Therefore, further structural analysis, especially on the group I S2Ps having extracytoplasmic PDZ domains, is essential for understanding the mechanism of

[1]Graduate School of Medical Life Science, Yokohama City University, 1-7-29 Suehiro-cho, Tsurumi-ku, Yokohama 230-0045, Japan. [2]Institute for Life and Medical Sciences, Kyoto University, 53 Shogoinkawahara-cho, Sakyo-ku, Kyoto 606-8507, Japan. [3]Graduate School of Science, University of Tokyo, 7-3-1 Hongo, Bunkyo-ku, Tokyo 113-0033, Japan. [4]Life Science Research Infrastructure Group, RIKEN SPring-8 Center, 1-1-1 Kouto, Sayo-cho, Sayo-gun, Hyogo 679-5148, Japan. [5]Institute for Protein Research, Osaka University, 3-2 Yamadaoka, Suita, Osaka 565-0871, Japan. [6]Life Science Center for Survival Dynamics, Tsukuba Advanced Research Alliance (TARA), University of Tsukuba, 1-1-1 Tennodai, Tsukuba, Ibaraki 305-8577, Japan. [7]Department of Antibody Drug Development, Tohoku University Graduate School of Medicine, 2-1 Seiryo-machi, Sendai, Miyagi 980-8575, Japan. [8]Department of Molecular Pharmacology, Tohoku University Graduate School of Medicine, 2-1 Seiryo-machi, Sendai, Miyagi 980-8575, Japan.
*Corresponding author. Email: nogi@yokohama-cu.ac.jp (T.N.); yhizukur@infront.kyoto-u.ac.jp (Y.H.); yakiyama@infront.kyoto-u.ac.jp (Y.A.)
†These authors contributed equally to this work.
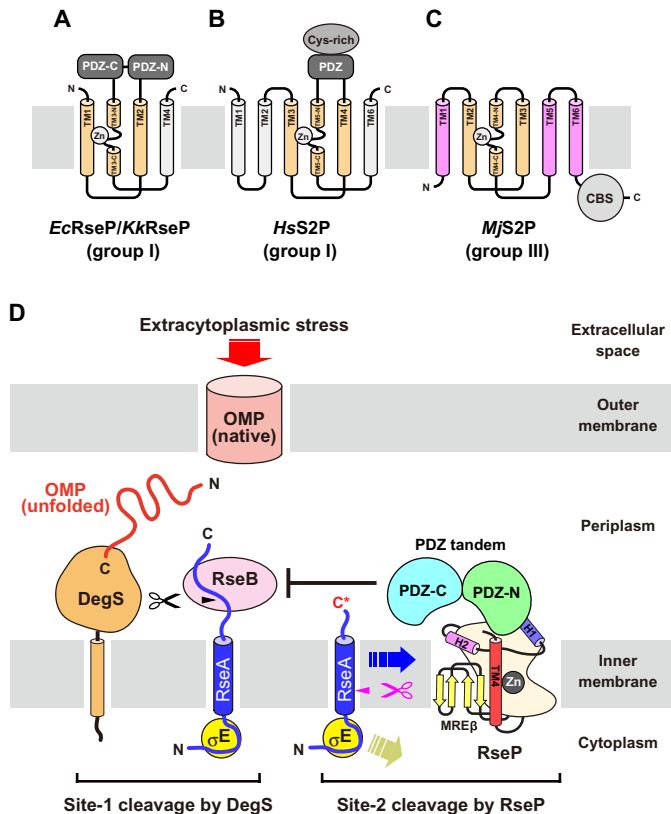
Fig. 1. Domain organization of the S2P family members and involvement of RseP in the *E. coli* extracytoplasmic stress response. The topology diagrams for (**A**) *Ec*RseP and *Kk*RseP of group I, (**B**) human S2P (*Hs*S2P) of group I, and (**C**) *Mj*S2P of group III, respectively. The three TM helices colored orange constitute a conserved catalytic core region. The group I S2Ps have a different number of PDZ domains. *Hs*S2P contains a Cys-rich region inserted into the PDZ domain. The group III S2Ps (e.g., *Mj*S2P) have a cystathionine-β-synthase (CBS) domain but no PDZ domain. Crystallographic analysis of *Mj*S2P suggests that TM1, TM5, and TM6 (light magenta) serve as the substrate entry gate where the close proximity between TM1 and TM6 forms a gate–closed state (*26*). TM1 and TM6 in *Mj*S2P are less or not conserved in *Hs*S2P and RsePs. (**D**) Extracytoplasmic stress causes accumulation of unfolded or denatured outer membrane proteins (OMPs) in the periplasm, together with dissociation of RseB from RseA. DegS, the *E. coli* counterpart of site-1 protease (S1P), is activated by interaction with the unfolded OMP and cleaves the periplasmic region of the anti–sigma factor RseA (site-1 cleavage). Subsequently, RseP performs intramembrane proteolysis of the DegS-cleaved form of RseA (site-2 cleavage), which leads to the activation of σ^E. The PDZ tandem of RseP was proposed to sterically hinder the entry of the full-length RseA complexed with RseB. In this study, structure-based mutational and cross-linking analyses have been conducted to address the question of how RseP accommodates the site-1–cleaved substrates using the PDZ tandem, the PDZ C-terminal (PCT) region including H1 and H2 helices, TM4, and the MREβ-sheet.

sequential cleavage and substrate accommodation in the intramembrane proteolysis by S2Ps.

Here, we began by performing x-ray crystallographic analysis on *Ec*RseP and its ortholog to produce the first atomic models for the group I subfamily of S2P. Specifically, we have elucidated their three-dimensional structures in complex with a peptide-mimetic inhibitor, which aided the design of mutational analyses to examine the binding mode of substrate TM segments. Furthermore, the observed structural differences between *Ec*RseP and the ortholog prompted us to examine the possibility of domain rearrangement in *Ec*RseP

during substrate accommodation and cleavage. The results provide crucial insights into the mechanism of the intramembrane proteolysis not only for S2Ps but also for the other families of intramembrane proteases that cleave the TM segments of substrates.
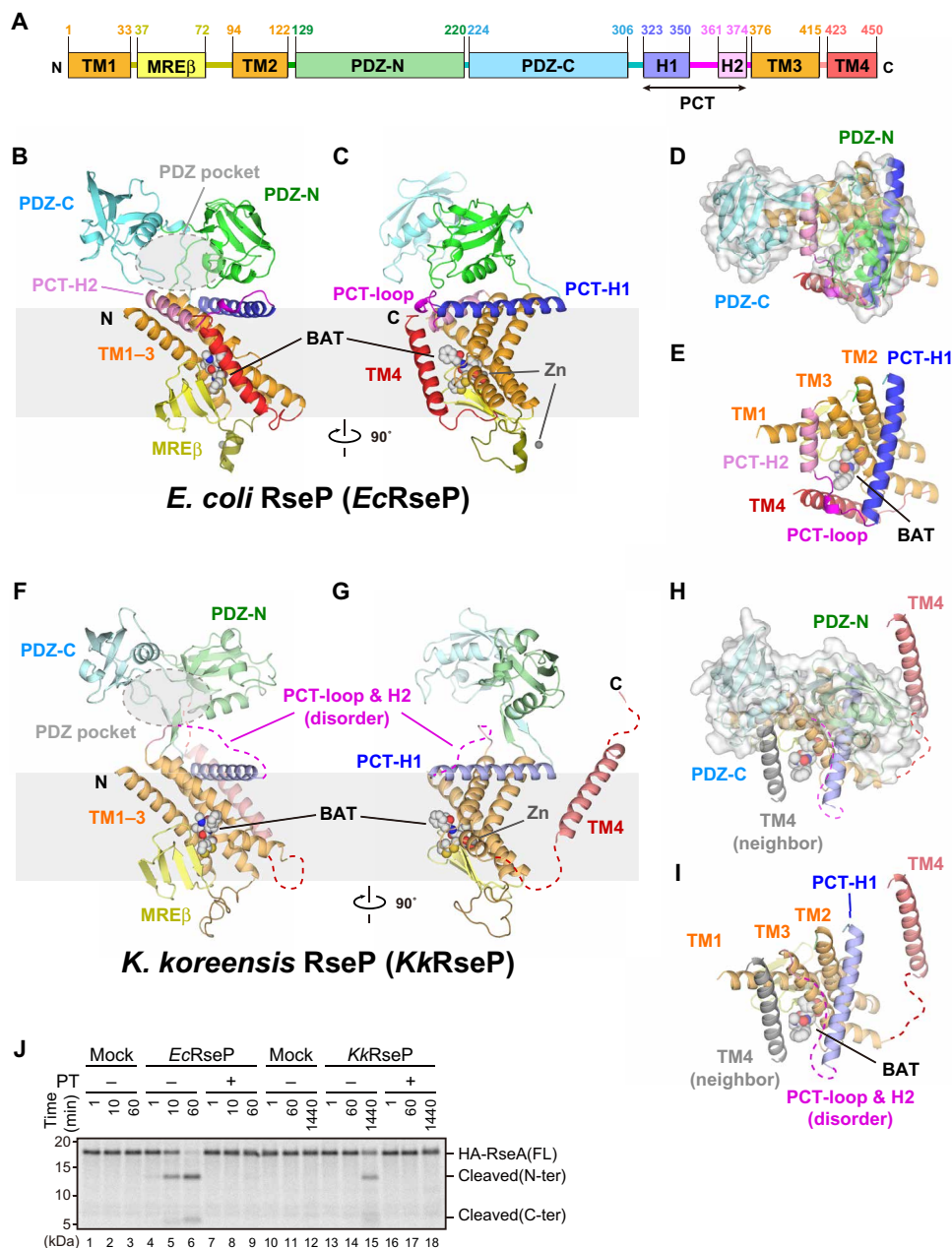
RESULTS

Crystallographic analysis of *Ec*RseP and *Kk*RseP

For structural analysis, we purified RseP from *E. coli* (*Ec*RseP) and its ortholog from marine bacterium *Kangiella koreensis* (*Kk*RseP) (fig. S1). *Kk*RseP restored the growth deficiency of *E. coli* rseP mutant cells (fig. S2A). In *E. coli*, *Kk*RseP cleaved an analog of its native substrate containing the TM segment from the *K. koreensis* RseA ortholog and substrate analogs for *Ec*RseP. Mutations to the putative *Kk*RseP active site impaired this cleavage activity (fig. S2, B and C). Furthermore, detergent-solubilized *Kk*RseP can cleave *E. coli* RseA, although with reduced activity as compared with *Ec*RseP (Fig. 2J). In this study, crystal structures of *Ec*RseP and selenomethionine (SeMet)–substituted *Kk*RseP were determined in complex with batimastat, an inhibitor for *Ec*RseP (Fig. 2, Table 1, and fig. S3) (*27*).

Overall structure of *Ec*RseP

The final model of *Ec*RseP (M1 to F447) is full length except for the three C-terminal residues and recombinant tag (Fig. 2, B to E). TM1 (M1 to C33) contains two zinc-coordinating His residues, H22 and H26 (fig. S4A). TM3 is divided by a loop-like bulge into two segments, TM3-N and TM3-C. TM3-C contains the third zinc-coordinating residue, D402 (fig. S4A). Besides the zinc ion in the active center, a second zinc ion was bound to H86 and H87 in the cytoplasmic region. However, its physiological role is currently unknown as H86A and/or H87A mutations did not affect the proteolytic activity (fig. S4, B to D, and table S5). *Ec*RseP was predicted to have two intramembrane β hairpins, the C1N loop (*25*) and the membrane-reentrant β loop (MREβ-loop) (*24*), between TM1 and TM2 (fig. S1). The corresponding regions are integrated into a four-stranded β sheet (hereafter referred to as the MREβ-sheet) (fig. S5, A and B). Strand 4 corresponds to the edge strand and forms one side of the substrate-binding site where its backbone makes direct contacts with batimastat (Fig. 3). These observations are consistent with our previous findings that proteolytic activity is reduced by introducing Pro mutations into the two strands closest to the active site as observed here, either into the N-terminal region of C1N (R39 to F44 corresponding to strand 1) or into the C-terminal region of the MREβ-loop (G67 to V70 corresponding to strand 4) (*25*). Similarly, substrate cleavage was strongly impaired in the G43A/I61G double mutant but not by either single mutation. In the crystal structure, G43 and I61 are proximal (G43 on the C1N loop and I61G on the MREβ-loop). *Mj*S2P also has a membrane-embedded β sheet (*26*), while its topology differs in strand order. However, strand 4 is still proximal to the active center (fig. S5, C and D), and the arrangement of the β sheet relative to the active center is the same as for the MREβ-sheet of *Ec*RseP. Together, TM1 to TM3 and the MREβ-sheet structurally align with their equivalents in *Mj*S2P.

A hydrophilic compartment for substrate binding and cleavage within the membrane is formed with substantial structure contributions from the MREβ-sheet (fig. S6). The edge strand of the MREβ-sheet, together with the conserved TM core region, forms a compartment that accommodates batimastat and the catalytic zinc ion. The interior of

京都大学
KYOTO UNIVERSITY

京都大学学術情報リポジトリ
KURENAI 紅
Kyoto University Research Information Repository

SCIENCE ADVANCES | RESEARCH ARTICLE

Fig. 2. Crystal structures of EcRseP and KkRseP. (**A**) Domain organization of EcRseP. The yellow rectangle labeled with MREβ indicates the MREβ-sheet. The rectangles labeled with H1 and H2 indicate PCT-H1 and PCT-H2, respectively. (**B** and **C**) Two views of the structure of full-length EcRseP. Polypeptide chains are shown as ribbon models. Batimastat (BAT) and zinc ions (Zn) are shown as sphere models. Each domain or motif is colored as in (A). (**D** and **E**) View of the structure of full-length EcRseP from an outside-in perspective relative to the membrane. The PDZ tandem is highlighted with a transparent surface in (D), while the PDZ tandem is removed to visualize the PCT region and the helix bundle of the TM domain in (E). (**F** to **I**) Structure of full-length KkRseP in the same views as that of EcRseP. In (H) and (I), the TM4 segment from the crystal packing neighbor is accommodated into the TM1-TM3 cleft and is shown in a gray ribbon model. (**J**) In vitro substrate cleavage assay with purified RseP proteins. ^{35}S-Met–labeled model substrate HA-RseA148 from cell-free synthesis was incubated at 37°C for the indicated periods with EcRseP (2.5 ng/μl; 50 nM), KkRseP (100 ng/μl; 2.0 μM), or enzyme buffer only (mock) plus 5 mM zinc chelator 1,10-phenanthroline (PT+) or 5% dimethyl sulfoxide (DMSO) (PT−) as indicated. Model substrate and cleavage products (labels, right) on a bis-tris SDS–polyacrylamide gel electrophoresis (SDS-PAGE) gel were visualized using a PhosphorImager. A representative result from three technical replicates is shown.

this compartment, which is separated from the lipid bilayer by TM4, is hydrophilic because of the presence of several charged or polar residues (K71, D74, R76, E78, R97, N108, S387, N394, H405, E412, Y428, S432, and the zinc-coordinating residues) and the exposed backbone of the edge strand (fig. S6, A and B). The previous

crystallographic analysis of MjS2P had also suggested that both the exposed backbone of the edge strand and the charged residues on the TM helices coordinate water in a channel to the active site (26). The MREβ-sheet also has several charged residues on the cytoplasmic side and likely excludes lipid molecules, assisting the

Table 1. Crystallographic data and refinement. Values in parentheses are for the highest-resolution shell. PDB, Protein Data Bank. a.s.u., asymmetric unit.

Datasets	*Ec*RseP	*Kk*RseP (#1)	*Kk*RseP (#2)
Data collection			
Space group	*P*1	*P*1	*P*2₁
Cell dimensions			
a, b, c (Å)	47.34, 56.12, 69.67	44.56, 49.78. 76.08	46.27, 40.80, 160.24
α, β, γ (°)	68.2, 74.6, 69.3	86.9, 79.2, 82.2	90, 91.6, 90
No. of molecules/a.s.u.	1	1	1
X-ray source	SPring-8 BL32XU	SPring-8 BL32XU	SPring-8 BL32XU
Wavelength (Å)	1.0000	0.9700	0.9700
Resolution limits (Å)	43.77–3.20 (3.31–3.20)	49.30–3.10 (3.21–3.10)	40.80–3.15 (3.26–3.15)
No. of unique reflections	10,129 (1,028)	11,493 (1,130)	10,675 (1,055)
Completeness (%)	99.7 (99.8)	99.8 (99.8)	99.6 (99.8)
Redundancy	8.4 (7.8)	135.8 (122.9)	72.0 (66.3)
$\langle I/\sigma(I)\rangle$	7.5 (1.1)	20.0 (1.4)	13.8 (1.5)
$R_{\text{p.i.m.}}$	0.098 (1.347)	0.038 (1.601)	0.081 (0.914)
CC (1/2)*	0.995 (0.417)	0.999 (0.821)	0.999 (0.602)
Refinement			
Resolution limits (Å)	43.76–3.20 (3.66–3.20)	40.91–3.10 (3.24–3.10)	40.55–3.15 (3.32–3.15)
R_{work}	0.2460 (0.2952)	0.2564 (0.4159)	0.2654 (0.3595)
R_{free}	0.3053 (0.3320)	0.2987 (0.4787)	0.2882 (0.4023)
No. of non-H atoms	3,478	3,230	3,252
Protein	3,444	3,197	3,219
Zn^{2+}	2	1	1
Batimastat	32	32	32
Average B factor (Å²)	94.52	92.30	91.49
Protein	94.60	92.50	91.35
Zn^{2+}	83.44	64.45	110.74
Batimastat	87.24	73.57	105.10
RMSD from ideality			
Bond length (Å)	0.002	0.002	0.002
Bond angle (°)	0.48	0.50	0.44
Ramachandran plot			
Favored (%)	93.92	95.01	92.12
Outlier (%)	0	0	0.74
PDB code	7W6X	7W6Y	7W6Z

*Correlation coefficient between intensities from random half-datasets.

hydrophilic compartment to recruit water molecules into the active center (fig. S6C). In addition, the cytoplasmic region following the edge strand may also contribute to substrate binding and cleavage. Many S2Ps, including those from both group I and group III, contain acidic residues in the region connecting the putative edge strand and the following TM region (fig. S1). Mutations of these acidic residues substantially reduced the proteolytic activity in the *Bacillus subtilis* group III S2P homolog SpoIVFB (*23*). In *Ec*RseP, most of the acidic residues in the cytoplasmic region downstream of the MREβ-sheet form salt bridges with the surrounding basic residues and contribute to the formation of the hydrophilic compartment while this cytoplasmic

region forms a small globular domain (fig. S6D). Our structural data also support that the acidic residues in this region are involved in binding substrate and/or recruiting water molecules to the active center.

The PDZ tandem protrudes into the periplasmic space (Fig. 2, B and C). The two PDZ domains form a pocket-like space (PDZ pocket) oriented toward the TM domain containing the active center (Fig. 2, B to D). As predicted in the previous study (*21*), the N-terminal residues of the PDZ C-terminal (PCT) region (P323 to T350) form an amphiphilic helix (PCT-H1) at the membrane surface (Fig. 2C). PCT-H1 leads to a loop region (the PCT-loop: G351 to G360) containing a short 3₁₀ helix (PCT-SH) (Fig. 2E and fig. S1). PCT-H1 and the

SCIENCE ADVANCES | RESEARCH ARTICLE
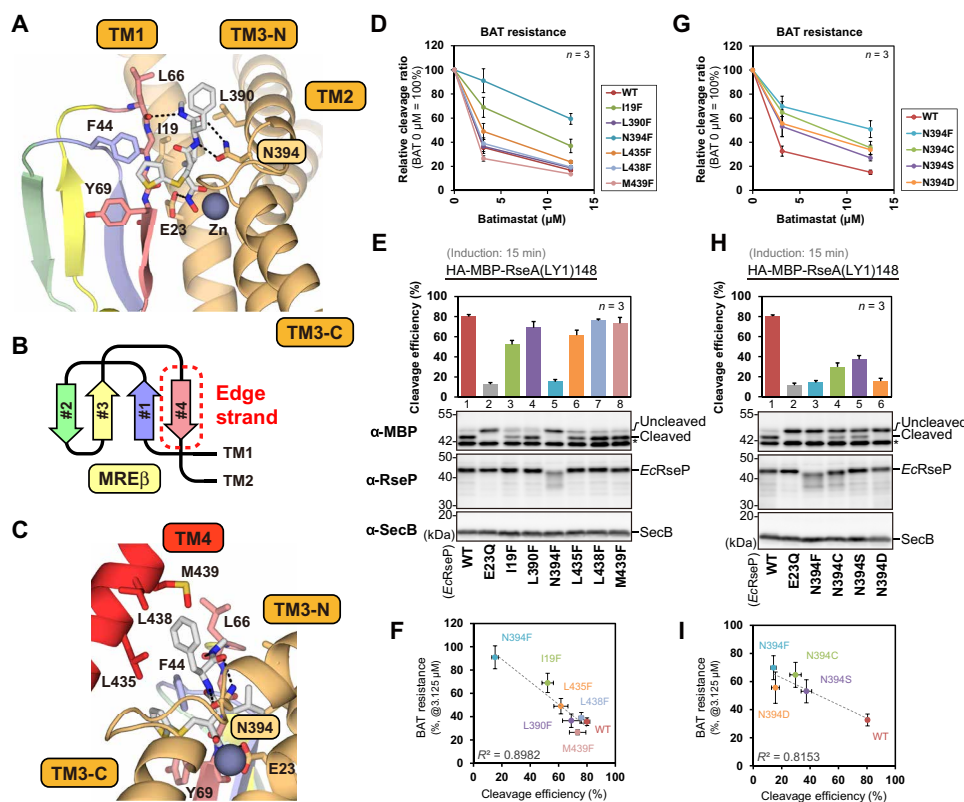
Fig. 3. Binding mode of batimastat to *Ec*RseP and dependence on residue N394. (**A**) Close-up view of the batimastat-binding site. Batimastat and the residues in direct contact with batimastat are shown as stick models. The four strands constituting the MREβ-sheet are shown in different colors. TM4 is omitted to visualize the binding site. (**B**) Topology diagram of the MREβ-sheet. (**C**) Interaction between TM4 and batimastat. (**D** and **G**) In vivo batimastat sensitivity assay. *E. coli* YH2902 cells harboring one plasmid for HA-MBP-RseA(LY1)148 (pYH124) and one for tagless *Ec*RseP (pYH825) or its variants were first treated with 0, 12.5, or 3.125 μM batimastat at 30°C for 10 min and then induced with 1 mM isopropyl-β-D-thiogalactopyranoside (IPTG) for 1 hour. The relative cleavage ratio was determined by quantitating the signal from immunoblots and comparing the value with that for the 0 mM BAT condition. Points and error bars represent the means ± SD from three biological replicates (see fig. S7 for the raw data). (**E** and **H**) In vivo substrate cleavage assay with short induction. YH2902 cells carrying two plasmids as in (D) and (G) were incubated with 1 mM IPTG for 15 min. The cleavage efficiency was determined as described in Materials and Methods. SecB serves as a loading control. An asterisk indicates endogenous maltose-binding protein (MBP). Bar plots and error bars represent the means ± SD from three biological replicates. (**F** and **I**) Scatterplots of the BAT resistances of the RseP mutants [relative cleavage ratio under 3.125 μM BAT concentration shown in (D) or (G)] against the cleavage efficiencies of the model substrate [shown in (E) or (H)].

PCT-loop make direct contacts with PDZ-N. The present structural analysis also showed that the C-terminal residues of PCT (P361 to L374) also form a helix (PCT-H2), which makes a sharp turn at the C-terminal end (G375) and leads to TM3-N (Fig. 2E). PCT-H2 is accommodated into a cleft formed between TM1 and TM3-N and is located just above the batimastat bound to the active center. In *Ec*RseP, TM4 (V423 to F447) interacts with the PCT-loop and PCT-H2 at the periplasmic side and covers the batimastat.

Binding mode of batimastat

The peptide-mimetic batimastat adopts an extended conformation and is flanked by the edge strand of the MREβ-sheet and TM3-N in *Ec*RseP (Fig. 3 and fig. S7A). The main chain of batimastat forms hydrogen bonds with the main chain of L66 on the edge strand and with the side chain of N394 on TM3. For the side chains of batimastat, the isobutyl group is oriented toward I19 in TM1 and L390 in TM3-N, while the thienyl group is close to both of the residues that were reported to interact with substrates, F44 of the conserved GFG motif (*25*) and Y69 on the edge strand of the MREβ-sheet (*24*). In addition, the phenyl group of batimastat forms van der Waals interactions with L435, L438, and M439 on TM4 (Fig. 3C).

On the basis of the structural data, we examined whether side chains could also affect inhibitor (and thereby substrate) accommodation in addition to the backbone interactions with the edge strand. I19N and I19F mutations to TM1 have been reported to reduce the sensitivity of *Ec*RseP to batimastat (*27*). We further introduced Phe mutations to the residues interacting with batimastat on TM3 and TM4 (L390 and N394 on TM3 and L435, L438, and M439 on TM4) and examined their effects on batimastat sensitivity. To eliminate the influence of the C-terminal tags on this analysis, we introduced these mutations into a tagless *Ec*RseP construct (Fig. 3D and fig. S7, B and C). In the wild type (WT), addition of 3.125 μM batimastat reduced the relative cleavage ratio of the substrate to 40%. At the same batimastat concentration with N394F, the relative cleavage ratio was only reduced to 90%. I19F also showed increased resistance to batimastat as reported (*27*). Furthermore, batimastat resistance seems to correlate negatively with the intrinsic proteolytic activity of the mutants in the absence of batimastat, particularly with a shorter induction of *Ec*RseP (Fig. 3, E and F). The N394F mutation with the strongest impact on batimastat resistance also reduced the proteolytic activity to a greater extent as compared to other mutations. Next, we introduced N394C, N394S, and N394D mutations to evaluate the

possibility that the reduced activity in N394F is ascribed to lower accumulation resulting from fold destabilization. We observed that all three mutants accumulated in *E. coli* but still showed substantial increase both in batimastat resistance and in reduction of proteolytic activity (Fig. 3, G to I, and fig. S7, D and E). In particular, the reduction of proteolytic activity for the isosteric mutation N394D indicates that hydrogen bonding via the amide group of the N394 side chain is critical for the cleavage. N394 may clamp a bound substrate at the active center as it interacted with the backbone of batimastat at the opposite side of the MREβ-sheet. In total, it is likely that the binding mode of batimastat partly reflects that of native RseP substrates. The substrate segments to be cleaved are thought to be extended by the strand addition, as proposed in our previous work (*24*), and shielded from the hydrophobic milieu of the lipid bilayer by the surrounding TM helices of RseP.

Overall structure of *Kk*RseP

*Kk*RseP produced two crystal forms with similar crystal packing (fig. S8, A to D). The two crystal structures of *Kk*RseP are almost identical with a root mean square deviation (RMSD) of 1.34 Å for 387 Cα atoms (fig. S8, E and F), excluding some disordered loops. The structures of individual domains in *Kk*RseP are similar to those in *Ec*RseP, including the binding mode of batimastat via the MREβ-sheet and side chain–backbone interactions with N387 (corresponding to N394 in *Ec*RseP) (Fig. 2, F to I, and fig. S9). However, the *Kk*RseP structures showed substantial differences in the domain arrangement relative to those in *Ec*RseP. For instance, the PDZ tandem is positioned further from the PCT region, and the C-terminal part of PCT (corresponds to the PCT-loop and H2 in *Ec*RseP) is disordered (Fig. 2, F, G, and I). Thus, *Kk*RseP adopts a PDZ-open conformation, while *Ec*RseP is in a PDZ-closed conformation. In addition, TM4 moves away from the domains forming the active center to interact with the cleft between TM1 and TM3-N in the crystal packing neighbor (Fig. 2, H and I, and fig. S10A). TM4 also interacts with the batimastat bound to the active center of the neighbor. The phenyl group of batimastat makes close contacts with V428 and L429 on TM4 (fig. S9B). In addition, residual electron density was observed close to PDZ-C. This electron density is most likely derived from the C-terminal residues of the tobacco etch virus (TEV) protease consensus sequence in the *Kk*RseP construct (fig. S10, A and B). As the two neighboring *Kk*RseP molecules in the crystal form an asymmetric dimer, it is probable that the accommodation of TM4 into the neighbor is an artifact of the crystal packing. However, the conformational difference between *Ec*RseP and *Kk*RseP raised the possibility that the PDZ tandem, the C-terminal part of PCT, and TM4 can rearrange without disrupting the TM core region. Such structural changes, if they occur, would likely affect the regulation of substrate accommodation.

Arrangement of the PDZ tandem in *Ec*RseP and *Kk*RseP on the cell membrane

To explore the possibility of domain rearrangement, we first examined the arrangement of the PDZ tandem in *Ec*RseP and *Kk*RseP in the spheroplast (i.e., on the cell membrane) using a methoxypolyethylene glycol 5000 maleimide (mal-PEG) accessibility assay. For *Ec*RseP, we introduced four single-Cys mutations to the PDZ tandem in the tagless construct to eliminate the impact of the C-terminal tags on the conformation of the PDZ tandem. Consequently, we observed that the Cys residue in A136C (located outside the PDZ pocket) was

efficiently modified with mal-PEG (~5 kDa). In contrast, the Cys residues in D163C, L167C, and I304C were modified only upon the addition of detergent (Fig. 4, A to C). In the crystal structure, L167 on PDZ-N makes direct contacts with PCT-H1, while D163 is deep in the PDZ pocket. I304 belongs to the carboxylate-binding loop of PDZ-C and is located inside the pocket. These results indicate that *Ec*RseP on the membrane adopts the PDZ-closed conformation as in the crystal structure where the PDZ pocket is sterically hindered by the bilayer and the PCT region. Next, we also examined the conformation of the PDZ tandem in *Kk*RseP on the cell membrane. To conduct the accessibility assay on *Kk*RseP without a C-terminal tag, we inserted an exogenous epitope, PA14 tag (*28*), into a β turn between K54 and H55 in the MREβ-sheet for antibody labeling. We confirmed that the resulting *Kk*RseP(54-PA14-55) and its four single-Cys mutants (P136C, E163C, F167C, and I302C) accumulated in *E. coli* and maintained proteolytic activity (fig. S11). If *Kk*RseP on the membrane adopts the PDZ-open conformation as in the crystal structure, then all of the four Cys mutants should be modified to some extent in the spheroplast. Nevertheless, although E163C (proximal to PCT) underwent substantial but rather low modification, F167C (proximal to PCT) and I302C (inside the PDZ pocket) were unmodified in the absence of detergent (Fig. 4, D to F). These results suggest that the two modification sites (F167 and I302) were inaccessible because of the closer proximity between the PDZ tandem and the PCT region in *Kk*RseP on the membrane, similar to what is observed in the crystal structure of *Ec*RseP (PDZ-closed) rather than that of *Kk*RseP (PDZ-open) (Fig. 4G). Thus, the PDZ-open conformation of *Kk*RseP in the crystal may be induced by the rearrangement of the PCT region or by the accommodation of TM4 from the crystal packing neighbor.

Importance of D446 on TM4 for substrate cleavage

We next explored the role of TM4 in substrate cleavage. Although TM4 is less conserved compared to the other three TM regions within the S2P family (*15*) (Fig. 5A), the binding mode of batimastat in *Ec*RseP suggests that TM4 contributes to the formation of the hydrophilic compartment around the active site (fig. S6, A and B). Hence, we prepared two *Ec*RseP mutants, ΔTM4 lacking the entire TM4 and C-terminal tail region (F426 to the C terminus) and ΔCTail lacking only the C-terminal tail region (D446 to the C terminus), and assessed the effect of the mutations on the cleavage. We observed that both ΔTM4 and ΔCTail did not complement the *Ec*RseP deficiency (Fig. 5B). Furthermore, both mutants virtually lost proteolytic activity, although ΔCTail exhibited residual activity (Fig. 5C). We next mutated conserved residues on TM4 to alanine (for G431, M439, D446, and R449) or serine (for A442) (Fig. 5, A and D, and fig. S12) to examine their contributions to the cleavage. We found that only the mutation to the highly conserved D446 (fig. S1) impaired complementation and proteolytic activity. As the carboxyl side chain of D446 is positioned for interaction with the electropositive N-terminal end of the helix dipole on PCT-H2 in the crystal structure, the interaction between D446 and PCT-H2 may be critical for the maintenance of the proteolytic activity (Fig. 5E). Analysis of additional D446 mutants showed that only D446E retained proteolytic activity (Fig. 5C and fig. S13), although its complementation activity was much lower than that of the WT (Fig. 5B). Notably, despite the absence of D446 in ΔCTail, this mutant exhibited a substantial proteolytic activity. This may be due to the presence of the terminal carboxyl group of N445 in the proximity of the N-terminal
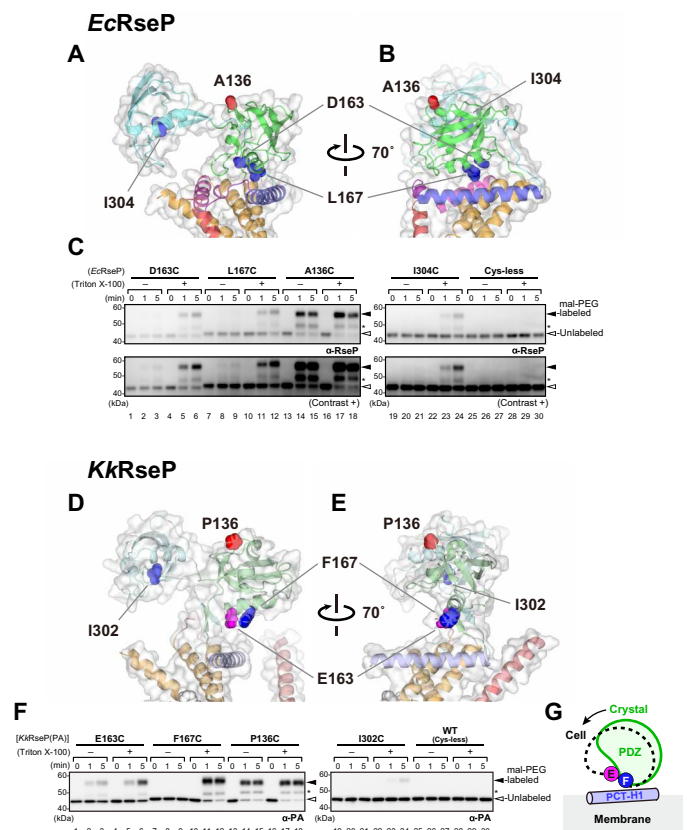
Fig. 4. mal-PEG accessibility assay for the PDZ tandem. (**A** and **B**) Mapping mutation sites onto the crystal structure of *Ec*RseP. The side chains of the mutated residues are shown as sphere models. The residue modified without detergent Triton X-100 (A136) is colored red, while the other residues colored blue were modified upon addition of the detergent. (**D** and **E**) Mapping mutation sites onto the crystal structure of *Kk*RseP, as in (A) and (B). The residue modified slightly without the detergent (E163) is colored magenta. (**C** and **F**) Mal-PEG accessibility assay for the *Ec*RseP and *Kk*RseP Cys mutants. Spheroplasts of KK374 cells carrying a plasmid encoding Cys-less *Ec*RseP (pYH835), *Kk*RseP with internal PA14 tag (pYH838), or one of their single-Cys mutants were treated with 1 mM mal-PEG in the presence or absence of 2% Triton X-100 at 4°C for the indicated periods. "Contrast +" indicates a signal-enhanced image. An asterisk indicates RseP derivatives modified with a minor mal-PEG component (*62*). A representative result from two biological replicates is shown. (**G**) Conformation of the *Kk*RseP PDZ tandem. In the crystal structure of *Kk*RseP, the PDZ tandem adopts an open conformation (green). However, the mal-PEG assay indicates that the *Kk*RseP PDZ tandem on the cell membrane adopts a relatively closed conformation (black dotted line), in which F167 (blue circle) is expected to be closer to the PCT-H1 (light-blue column). The partial modification of E163 (magenta circle) without detergent indicates that the *Kk*RseP PDZ tandem is not as close to the PCT region as the *Ec*RseP PDZ tandem both in the crystal and on the cell membrane.

end of the helix dipole. In total, the above mutational analysis revealed a previously unrecognized importance to substrate cleavage for TM4 and that an Asp at position 446 is most ideal for this function in the native context. One possibility is that the electrostatic interaction between PCT-H2 and D446 is structurally important for the formation of the hydrophilic compartment that accommodates the substrate. Another possibility is that this interaction is important because substrate accommodation requires the coordinated structural rearrangement of the PCT-H2 and TM4 observed between the *Ec*RseP and *Kk*RseP structures.

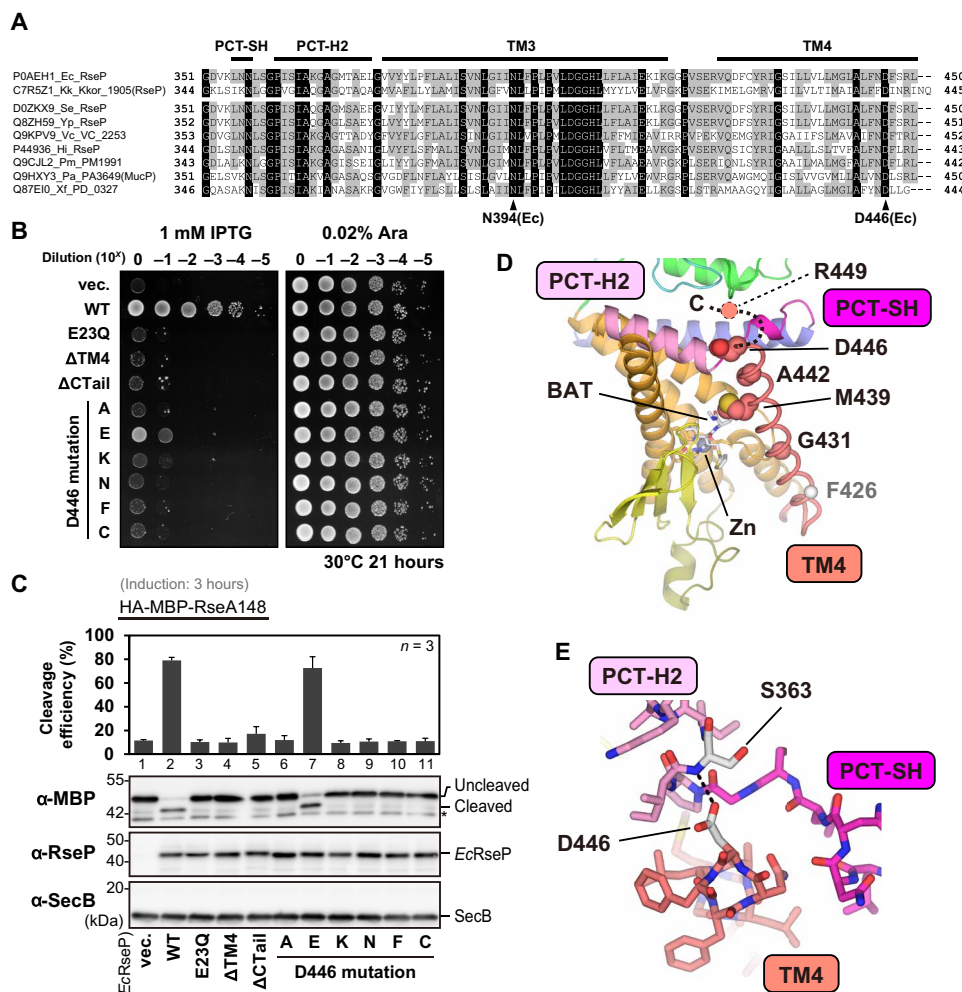## Involvement of PCT-H2 in the substrate cleavage

To examine whether the conformational rearrangement of PCT-H2 is involved in the substrate cleavage, we first performed Cys-scanning mutagenesis on PCT-H2 and the adjacent region (T350 to P381) to examine the mobility of PCT-H2 by a modified version of our accessibility assay with 4-acetamido-4′-maleimidylstilbene-2,2′-disulfonate (AMS) as the probe. AMS, a soluble thiol-alkylating reagent, reacts with Cys residues exposed to the aqueous milieu. We observed that all the Cys residues on PCT-H2 were modified at comparable levels in the spheroplast (fig. S14), although some residues—such as P361, I364, A365, A368, G369, and A372—are expected to be modified less frequently if PCT-H2 is fixed in the cleft between TM1 and TM3 as in the crystal structure. Hence, PCT-H2 is thought to be mobile in *Ec*RseP on the cell membrane. In contrast, Y379, L380, and P381 on TM3 showed low AMS modification in the spheroplast. The low AMS accessibility of these three residues is consistent with burial in the hydrophobic region of the lipid bilayer, as predicted on the basis of the crystal structure. Furthermore, we also examined the proteolytic activity of the Cys mutants and found that only G360C and G375C reduced the proteolytic activity (Figs. 5A and 6, A and C, and fig. S15). Considering the high conservation of the two Gly residues flanking both ends of PCT-H2, these results suggest that the proper positioning of PCT-H2 is important for the substrate cleavage.

Subsequently, we also tested whether PCT-H2 is involved in the regulation of the sequential cleavage. We performed a LacZ reporter assay on the Cys mutants to monitor σ^E activation resulting from deregulated cleavage of intact RseA without the prior site-1 cleavage by DegS. We found that L355C, L358C, and I362C deregulate *Ec*RseP, although the extent of deregulation was smaller than that from L151P, a known deregulated mutant on PDZ-N (Fig. 6, B and C) (*29*). We also examined trypsin susceptibility of the three mutants on the cell membrane as a proxy for stability. As reported previously, L151P showed increased trypsin susceptibility (lanes 5 to 8; fig. S16) probably because this mutation disrupts the folding of PDZ-N (*20*). In contrast, almost no degradation was observed for the other mutants or for WT RseP (fig. S16). We also observed increased conformational flexibility in the PDZ-C domain of L358C using negative-stain electron microscopy (EM) (figs. S17 and S18), suggesting that the L358C mutation can deregulate *Ec*RseP by altering the arrangement of the PDZ tandem without destabilizing the individual PDZ domains. These results indicate that the proper positioning and mobility of PCT-H2 are also important for the regulated sequential cleavage of substrates and likely affect the positioning of TM4.

Conformational changes of the PCT region and PDZ tandem during substrate cleavage

Several lines of evidence from this study raised the possibility that the PDZ tandem and PCT region, probably in conjunction with TM4, undergo structural changes to accommodate the substrate into the active center for cleavage. Our previous in vivo photocrosslinking experiment using *p*-benzoyl-L-phenylalanine (*p*BPA) indicated that buried residue T341 on PCT-H1 is accessible to RseA (*21*). We therefore performed an intramolecular cross-linking experiment to test whether the proteolytic activity of *Ec*RseP is affected by immobilizing the PCT region and/or the PDZ tandem (Fig. 7, A and B). In this assay, *Ec*RseP mutants having two Cys mutations were first expressed under isopropyl-β-D-thiogalactopyranoside (IPTG) induction, then the cells were washed, and disulfide cross-linking was

Fig. 5. Involvement of TM4 in the substrate cleavage and dependence on residue D446. (**A**) Sequence alignment of the C-terminal regions of RseP orthologs from γ-proteobacteria. Ec, *E. coli*; Kk, *K. koreensis*; Se, *Salmonella enterica* serovar Typhimurium; Yp, *Yersinia pestis*; Vc, *Vibrio cholerae*; Hi, *Haemophilus influenzae*; Pm, *Pasteurella multocida*; Pa, *Pseudomonas aeruginosa*; Xf, *Xylella fastidiosa*. Conserved (100% match) and similar (≥50% match) residues are boxed in black and gray, respectively. (**B**) Complementation assay. Cultures of *E. coli* KK31 cells carrying plasmids for *Ec*RseP under the *lac* promoter (pYH825) or its variants were spotted on L agar plates containing IPTG or L-arabinose. A representative result from three biological replicates is shown. ΔTM4 and ΔCTail indicate the F426amber and D446amber mutations, respectively. (**C**) In vivo cleavage assay with long induction. KA306 cells harboring one plasmid for HA-MBP-RseA148 (pKA65) and one for *Ec*RseP (pYH825) or its variants were grown for 3 hours with 1 mM IPTG and 1 mM adenosine 3′,5′-cyclic monophosphate (cAMP). The cleavage efficiency was determined as in Fig. 3E. Bar plots and error bars represent the means ± SD from three biological replicates. (**D**) Conserved residues on TM4. The residues mutated to alanine or serine in fig. S12 are shown as spheres. A disordered region containing R449 is indicated by a dotted line. (**E**) Specific interaction between D446 and PCT-H2. TM4, PCT-SH in the PCT-loop, and PCT-H2 are shown as stick models in salmon, magenta, and pink, respectively. D446 interacts with the electropositive N-terminal end of the PCT-H2 helix dipole where the side chain of D446 and the main-chain N—H group of S363 (each in white) form a hydrogen bond.

induced with an oxidizing agent, diamide. As a control, we performed the same procedure but replaced the diamide with a reducing agent, dithiothreitol (DTT). Last, a model substrate was induced with arabinose, and cleavage was monitored with an immunoblot assay. In this cross-linking experiment, the Cys-less *Ec*RseP (indicated as WT* in Fig. 7A) cleaved the substrate efficiently under both oxidizing and reducing conditions, while the active site mutant E23Q exhibited essentially no proteolytic activity under these conditions, indicating that the diamide and DTT treatments had little impact on the proteolytic activity. We induced cross-linking between PCT-H2 and TM1 (D7C-K366C and S10C-G369C) by treatment with the oxidizing reagent diamide and then confirmed the cross-link formation by observing the oxidization-dependent mobility shift of

RseP on SDS–polyacrylamide gel electrophoresis (PAGE). We actually observed that cross-linking reduced the substrate cleavage efficiency (Fig. 7A), supporting the model that PCT-H2 moves out of the cleft between TM1 and TM3-N to accommodate the substrate. We also observed a reduction in the substrate cleavage efficiency for the other double-Cys mutants, but we detected no substantial mobility shift for them (lanes 9 to 16; Fig. 7A). Despite the lack of band shift, we conclude that both the I173C (PDZ-N)/K347C (PCT-H1) and the D205C (PDZ-N)/S359C (PCT-loop) mutants are cross-linked because neither could be modified at the introduced Cys residues with a sulfhydryl-specific reagent (mal-PEG) after pretreatment with the oxidizing reagent diamide (fig. S19). For the other two mutants, we could not unambiguously correlate the reduction in the substrate
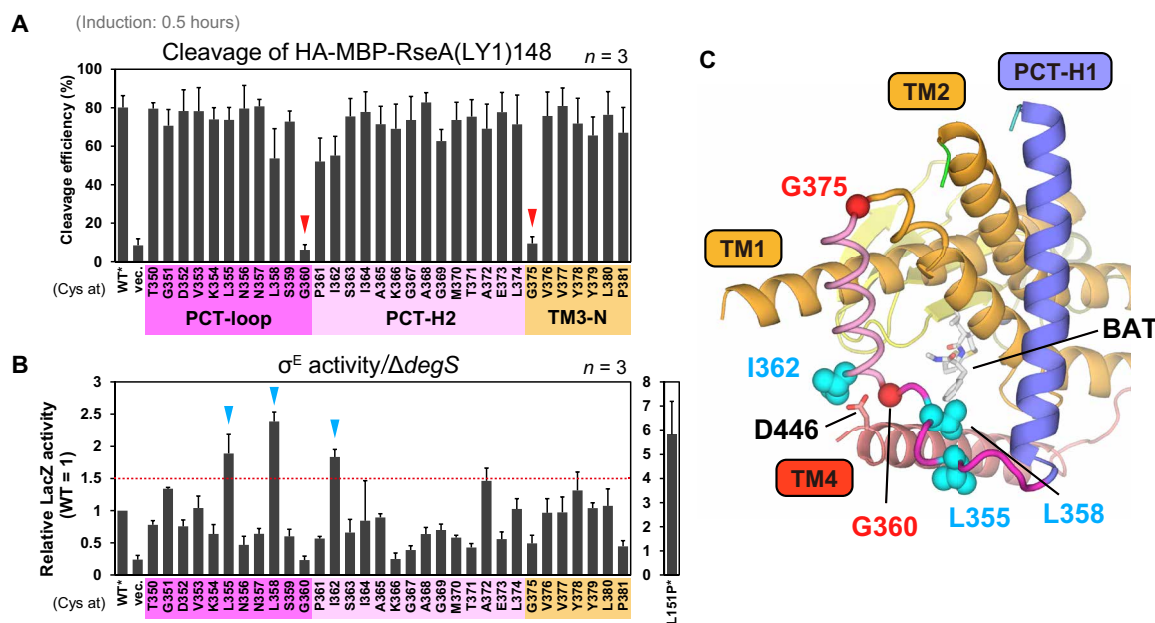
Fig. 6. Cysteine-scanning mutagenesis analysis of the PCT-H2 and the adjacent regions. (**A**) Substrate cleavage with short induction. *E. coli* KK211 (Δ*rseA* Δ*rseP*) cells harboring one plasmid for HA-MBP-RseA(LY1)148 (pYH20) and one for a variant of *Ec*RseP(Cys-less)-His$_6$-Myc (pTM132) were grown at 30°C in M9-based medium for 2.5 hours and further incubated for 0.5 hours with 1 mM IPTG and 5 mM cAMP. The cleavage efficiency was determined as in Fig. 3E (see fig. S15 for the raw data). Bar plots and error bars represent the means ± SD from three biological replicates. The region of each mutation is indicated by color (magenta, pink, and gold) and label. (**B**) DegS-independent σ^E activity of cells expressing RseP Cys mutants. Cells of *rpoH*P3-*lacZ* reporter strain AD2473 (Δ*degS* Δ*rseP*) harboring pSTD343 (*lacI*) and a plasmid for a variant of *Ec*RseP(Cys-less)-His$_6$-Myc (pTM101) were grown for 5 hours in L medium containing 0.1 mM IPTG and 1 mM cAMP. The measured LacZ activities are normalized as the ratio to the activity for the reporter strain expressing WT RseP (WT). The bar plot shows the means ± SD from three biological replicates. Red dashed line indicates the threshold for deregulated cleavage of intact RseA by the RseP Cys mutants. The previously isolated L151P mutant (right) shows high LacZ activity characteristic of deregulation. WT* and L151P* indicate Cys-less derivatives of WT and L151P RseP, respectively. (**C**) Mapping mutations on the *Ec*RseP model. Residues where the Cys mutation impaired the proteolytic activity are indicated with red sphere models. Residues where the Cys mutations caused deregulation are indicated with cyan sphere models.

cleavage efficiency with the formation of an intramolecular disulfide bond due to the diamide-dependent destabilization (D171C/S343C) or uncertainty regarding the cross-link formation (E203C/K354C). Collectively, the results of the cross-linking experiments support a model in which the PDZ tandem and the PCT region rearrange to accommodate the substrate for cleavage. In *Kk*RseP, the cleft between TM1 and TM3-N accommodates the TM4 from the crystal packing neighbor. We inferred that the bound TM4 might mimic the substrate and tested this prediction in an intermolecular photocross-linking experiment with *Ec*RseP and RseA. As anticipated, *p*BPA introduced at the position of Y378 on the cleft (Fig. 7B) is accessible to RseA in vivo (Fig. 7C and fig. S20), which also indicates a rearrangement of PCT-H2 during substrate accommodation.

DISCUSSION

In this study, we successfully determined the crystal structures of *Ec*RseP and *Kk*RseP as the first experimental structures for S2Ps with extracytoplasmic PDZ domains (group I). The structural features not only coincide with the previously proposed models but also provide new insights into the substrate accommodation mechanism. Specifically, the substrate discrimination and accommodation by *Ec*RseP are presumed to be regulated by three processes: size exclusion, gating, and unwinding (Fig. 8).

Previous structural and mutational analyses have proposed that the PDZ tandem serves as a size exclusion filter to regulate the sequential cleavage of the substrates (*20*). It was also proposed that PCT-H1 is involved in the size exclusion as an adapter (*21*). Furthermore, most point mutations that deregulate sequential cleavage have been located in the PDZ-N domain (*29*). On the basis of trypsin susceptibility, those deregulated mutations are presumed to cause large structural changes or unfolding of PDZ-N (*20*). The present crystallographic analysis of *Ec*RseP has shown that the PDZ-C domain protrudes in front of PCT-H2 to lie above the active center and thus appears to sterically hinder entry for substrates with a bulky periplasmic domain (Fig. 2, B to D). In addition, the PDZ-N domain makes direct contacts with the PCT-H1 in *Ec*RseP. Thus, the unfolding of the PDZ-N domain should destabilize the interaction between PDZ-N and PCT-H1, which may also perturb the geometry of size exclusion filter to deregulate its function. The Cys-scanning mutagenesis in this study further demonstrated that the PCT-loop and PCT-H2 also regulate the sequential cleavage (Fig. 6B). The EM analysis also suggested that the mutation to the PCT-loop region (L358C) causes deregulation through fluctuations in the orientation of the PDZ-C (fig. S18). These observations indicate that the PDZ-N domain and the PCT region serve as a scaffold to place the PDZ-C domain in a position to perform the size exclusion function. A similar substrate discrimination mechanism was proposed for γ-secretase where nicastrin regulates substrate entry by steric hindrance via a bulky extracytoplasmic domain (*30*).

Moreover, the present study indicates that a domain rearrangement occurs during the substrate accommodation and cleavage. On the basis of the modification and cross-linking analyses, we infer that the PDZ tandem, PCT-H2, and TM4 in *Ec*RseP serve as a gate for substrate entry. We anticipate that *Ec*RseP on the cell membrane is
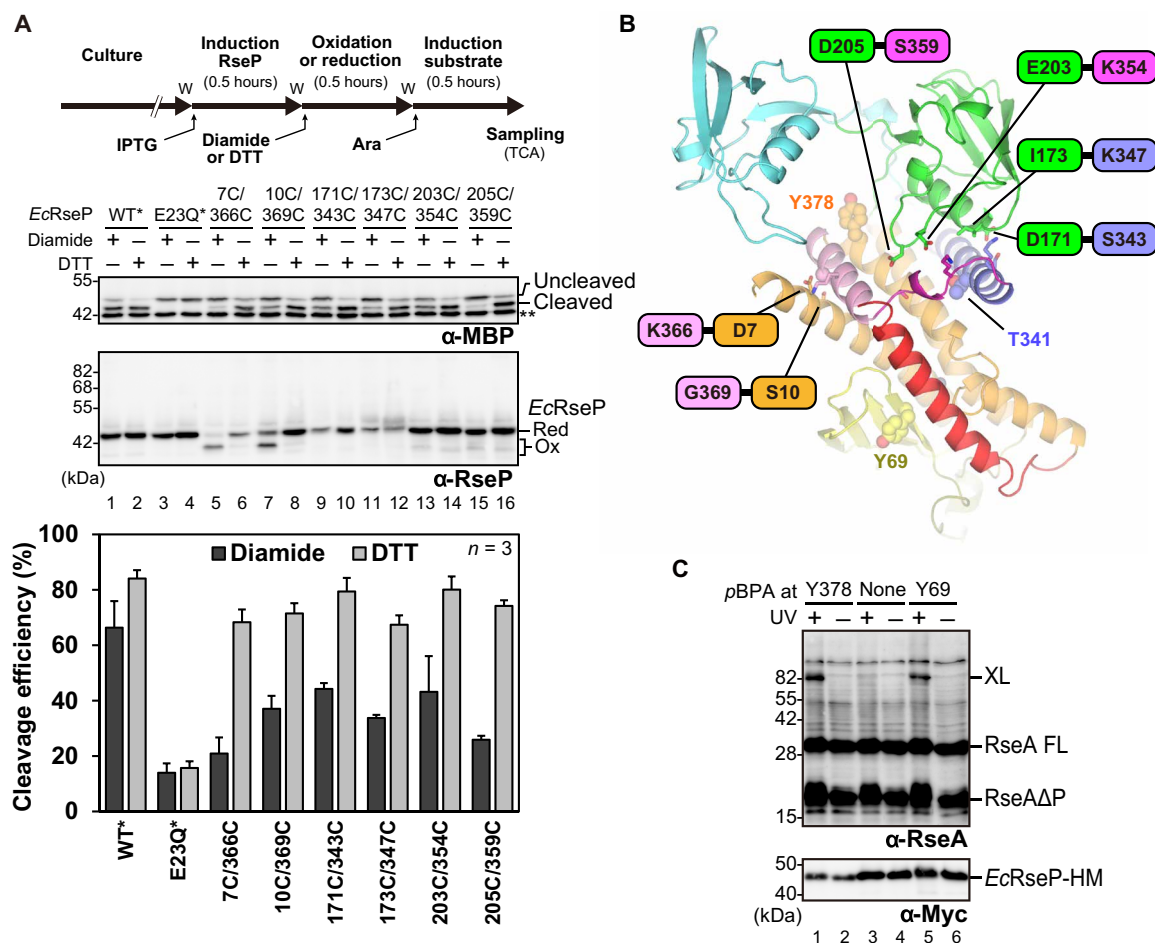
Fig. 7. Cross-linking experiments to examine the structural change during substrate cleavage. (A) In vivo proteolytic activity for *Ec*RseP after domain immobilization by disulfide cross-linking. AD2544 cells harboring an IPTG-inducible plasmid for *Ec*RseP (pYH835) or its variants and an arabinose-inducible plasmid for HA-MBP-RseA(LY1)148 (pTM949) were first induced with 5 mM IPTG and then treated with 5 mM diamide or 10 mM DTT. Time-course diagram is shown at the top where "w" indicates a cell wash step. After washing the cells, substrate expression and cleavage were induced with 0.02% ʟ-arabinose for 0.5 hours. The cleavage efficiency was determined as in Fig. 3E. Bar plots and error bars represent the means ± SD from three biological replicates. WT* and E23Q* indicate Cys-less derivatives of WT and E23Q RseP, respectively. Double asterisk indicates endogenous MBP. **(B)** Introduction of intramolecular cross-links. Six pairs of engineered Cys are indicated by a label, and their side chains are shown as stick models. Residues where the introduced *p*BPA was cross-linked with RseA are shown with sphere models. **(C)** In vivo photocrosslinking between *Ec*RseP(Y378*p*BPA) and RseA. KA418 (*rseA*⁺)/pEVOL-pBpF cells with pKA52 encoding RseP(E23Q)-His₆-Myc (none) or pKA52 derivatives having an amber mutation at the position of Y378 or Y69 were cultured and ultraviolet (UV)–irradiated as indicated. XL indicates the cross-linked products between RseP-HM and RseA. RseA FL and RseAΔP indicate the full-length and the DegS-cleaved form of RseA, respectively. RseP(Y69*p*BPA) with *p*BPA on the edge strand of the MREβ-sheet was used as a positive control for cross-linking. A representative result from three biological replicates is shown.

in equilibrium between the "gate-open" and "gate-closed" conformations. The AMS modification analysis indicates that PCT-H2 is mobile on the *E. coli* cell membrane. After the site-1 cleavage in the extracytoplasmic region, the substrate passes through the size exclusion filter to access the TM domain of *Ec*RseP. The substrate TM segment is thought to enter the active center when PCT-H2 and TM4 move away together, linked by the electrostatic interaction between the PCT-H2 backbone and conserved residue D446. On the basis of the intramolecular cross-linking analysis, the PDZ tandem is also thought to reorient relative to the PCT region during the substrate accommodation, whereas the PDZ pocket is still inaccessible enough to maintain the size exclusion function. The gating mechanisms are also presumed to exist not only in the S2P family but also in the other intramembrane proteases such as bacterial rhomboid GlpG (*31*, *32*) and γ-secretase (*33*), a member of the

presenilin/SPP family. In addition, it was proposed that *E. coli* rhomboid GlpG has an "interrogation site" for substrates in addition to a "scission site" to discriminate the substrates from nonsubstrates (*34*). As the cleavage efficiency in *Ec*RseP differs depending on the substrate, the proposed gating mechanism may also contribute to the substrate interrogation.

After the gate opening for the substrate accommodation, the substrate cleavage segments should bind with the edge strand via strand addition. We anticipate that the gate returns to a relatively closed conformation to shield the substrate TM segment from the hydrophobic milieu and to form a hydrophilic compartment around the active site for hydrolysis. Furthermore, our present structural analysis on *Ec*RseP complexed with batimastat indicates the importance of the conserved residue N394 in the substrate binding and cleavage. We previously observed that the *Ec*RseP(N394C) mutant
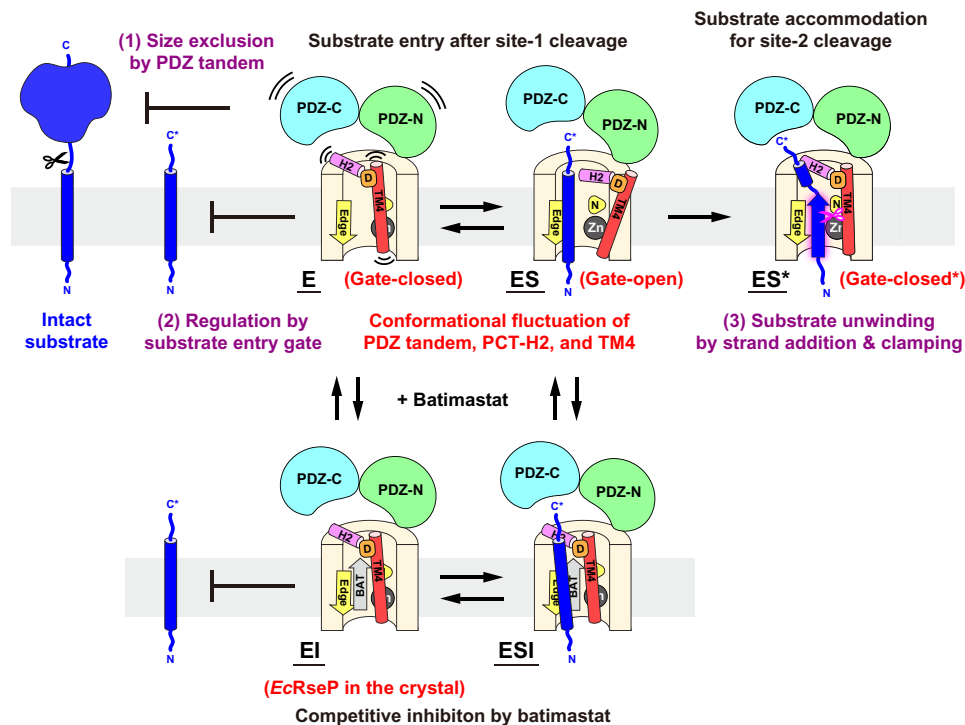
Fig. 8. Proposed mechanism for substrate accommodation and cleavage in *Ec*RseP. The substrate accommodation by *Ec*RseP is thought to be regulated by three processes. (**1**) Size exclusion process: The PDZ tandem restricts the entry of bulky intact substrates. After the site-1 cleavage, the size-reduced substrates become accessible to the TM domain of *Ec*RseP. (**2**) Gating process: The PDZ tandem, PCT-H2, and TM4 serve as a gate to regulate the substrate entry into the active center. In the gate-closed conformation (labeled the E state), the active center is covered by the PDZ tandem, PCT-H2, and TM4 and is inaccessible to the substrate TM segment. The present study suggests that the PDZ tandem is separated from the PCT region upon substrate binding (labeled the ES state). In this gate-opening movement, PCT-H2 and TM4 are also thought to move away from the active center while maintaining an electrostatic interaction via the conserved residue D446 (indicated in orange). (**3**) Unwinding process: The TM segment of the substrate is extended by the edge strand of the MREβ-sheet and clamped by the conserved residue N394 (indicated with a yellow round triangle) to promote the cleavage (labeled the ES* state). We anticipate that the gate adopts a relatively closed conformation (labeled "Gate-closed*") again to shield the substrate TM segment from the hydrophobic milieu. The crystal structure of *Ec*RseP with batimastat (gray arrow labeled "BAT") is thought to correspond to the EI state. The crystal structure of *Kk*RseP with batimastat may partly reflect the ESI state, in which TM4 of the crystal packing neighbor mimics the substrate TM segment.

showed no detectable cross-linking to Cys residues engineered into the TM segments of RseA derivatives. Thus, we inferred that N394 might not directly interact with RseA (*35*). However, our present crystallographic analysis demonstrated that the N394 side chain formed hydrogen bonds with the backbone of batimastat. Although the structure of the *Ec*RseP-substrate complex remains unsolved, the present mutational analysis prompted us to propose an alternative model in which N394 directly interacts with the backbone of the substrate TM segments to stabilize a cleavage-susceptible substrate conformation. Thus, the failure to cross-link between the *Ec*RseP(N394C) mutant and the RseA TM segment might be ascribed to the reduced affinity of this mutant to the substrate. We also observed that the N394C mutation reduced the affinity for the RseA TM segment in the coimmunoprecipitation assay (*35*). The residue corresponding to *Ec*RseP N394 in the *B. subtilis* homolog SpoIVFB (N129) has been shown to be important for substrate binding and cleavage. The SpoIVFB(N129C) mutant was disulfide cross-linked with coexpressed substrate mutants having a Cys residue in their TM segment, albeit with low efficiency (*36*), indicating the proximity of N129 to the bound substrate TM segment. In addition, the N129A mutation reduced the cross-linking efficiency of SpoIVFB with its substrate and reduced substrate cleavage (*36–38*), supporting the conclusion that N129 also stabilizes the bound substrate. Because

SpoIVFB is a group III S2P, this interaction may be common across diverse S2Ps. Furthermore, clamp-like interactions with unwound substrates appear to exist across the intramembrane proteases. The cryo-EM analysis of γ-secretase classified as an aspartic protease showed that substrate binding induces the formation of a β sheet in the TM region of presenilin (Fig. 9, A and B) (*33*, *39*). The β sheet binds with the substrate fragment via strand addition. In γ-secretase, the PAL motif is located on the opposite side of the β sheet like a clamp for the substrate. For the serine protease Rhomboid family, crystallographic analysis of *E. coli* GlpG in complex with substrate-derived inhibitors revealed that two loops connecting the TM helices (the L3 and L5 loops) sandwiched the peptide backbone of the inhibitor in an extended conformation (*40*). In the cocrystal structures, it appeared that L3 formed a parallel β sheet with the inhibitor, while L5 clamped it via backbone hydrogen bonds (Fig. 9, C and D). Furthermore, GlpG was also reported to capture a substrate peptide via the same backbone interactions with the L3 and L5 loops (*31*). Despite the difference in the catalytic mechanism, unwinding the TM helix into a strand conformation and stabilizing the bound substrate with a clamp structure seem to be common features in the intramembrane proteolysis of helical TM spans. Structure determination of substrate-bound and substrate-unbound forms of RseP or the group I S2Ps will deepen our understanding of the substrate
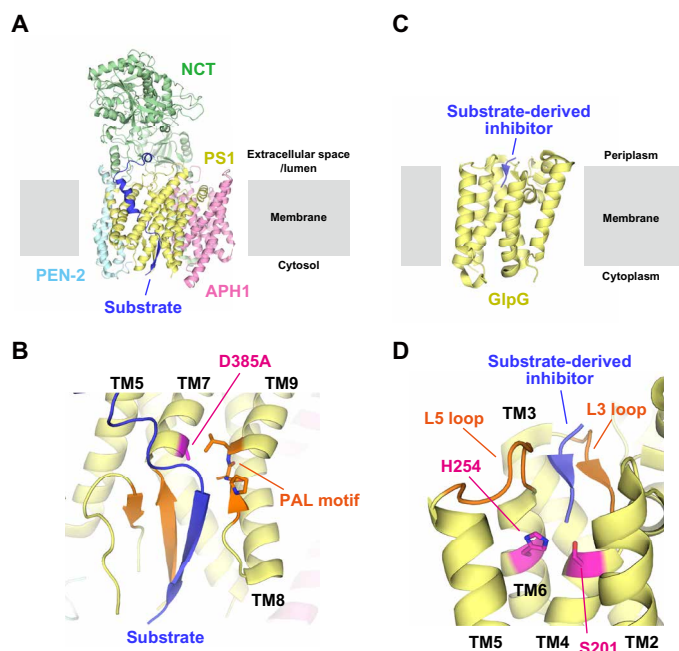
Fig. 9. Substrate unwinding modes in intramembrane proteases. (**A** and **B**) Cryo-EM structure of human γ-secretase in complex with the Notch fragment (PDB ID: 6IDF) (*33*). (A) γ-Secretase is composed of four subunits: presenilin 1 (PS1), nicastrin (NCT), anterior pharynx-defective 1 (APH1), and presenilin enhancer 2 (PEN-2). The Notch fragment indicated by "Substrate" in blue is accommodated in the catalytic subunit PS1. (B) Close-up view around the active site. In this structure, the active site residue D385 was mutated to alanine as highlighted in magenta. The C-terminal region of Notch is unwound by forming a hybrid β sheet with β strands (orange) in the cytosolic loop between TM6 and TM7 of PS1. The PAL motif between TM8 and TM9, highlighted with stick models, appears to fix the Notch fragment as a clamp. (**C** and **D**) Crystal structure of *E. coli* GlpG in complex with the substrate-derived inhibitor (PDB ID: 4QO0) (*40*). (C) GlpG has six TM helices and accommodates the peptide-mimetic inhibitor highlighted in blue in the cavity formed at the periplasmic side. (D) Close-up view around the active site. S201 and H254, highlighted in magenta, form the active center. The periplasmic L3 loop between TM3 and TM4 as well as the L5 loop between TM5 and TM6 (orange) sandwich the inhibitor where L3 forms a parallel β sheet with the inhibitor. L5 also appears to clamp the backbone of the inhibitor.

cleavage mechanism conserved across the intramembrane proteases and aid the development of strategies for regulating proteolytic activity in the membrane to prevent off-target or promiscuous cleavage.

MATERIALS AND METHODS
Construction of expression plasmids for structural analysis

A pUC118-based plasmid was constructed to produce *Ec*RseP for structural analysis. The resulting plasmid, designated as pNY1452, carried a gene encoding the WT full-length *Ec*RseP fused with a C-terminal tag containing the TEV consensus sequence, a His$_8$ tag, a Myc epitope, and a PA tag (*41*): -GT-ENLYFQG-G-HHHHHHHH-I-EQKLISEEDL-GVAMPGAEDDVV. For negative-stain EM, an expression plasmid for the L358C mutant, designated as pNY1550, was constructed from pNY1452 by the inverse polymerase chain reaction (PCR) method.

In parallel, we also searched for RseP orthologs suitable for structural analysis. Genes of 14 orthologs were amplified using genomic DNA obtained from the Japan Collection of Microorganisms

(RIKEN, Microbe Division) and subcloned into Nde I and Xho I sites of a modified pET-21b vector. Using the constructed plasmids, the orthologs were produced with a C-terminal tag containing the TEV consensus sequence and a His$_8$ tag: -LESSG-ENLYFQG-QFTS-HHHHHHHH. To examine the production level and dispersity, the orthologs produced in small-scale culture were subjected to detergent screening with fluorescence-detection size exclusion chromatography (FSEC) after the C-terminal His$_8$ tag was labeled using a peptide-based multivalent nitrilotriacetic acid (NTA) fluorescent probe, P3NTA. From the screen, an ortholog Kkor_1905 from *K. koreensis* str. DSM 16069 (*Kk*RseP; UniProtKB: C7R5Z1), a Gram-negative bacterium isolated from seawater of the tidal flat (*42*), was selected as a promising candidate for structural analysis. The expression plasmid carrying the *Kk*RseP gene without codon optimization was designated as pNY1432. The highest yield of monodisperse *Kk*RseP sample was obtained with an optimized preparation using *n*-dodecyl-β-ᴅ-maltoside (DDM) supplemented with cholesteryl hemisuccinate (CHS). The strains and plasmids used in the structural analysis including the procedures described below are summarized in tables S1 and S2.

Production and purification of full-length *Ec*RseP and *Kk*RseP

*Ec*RseP was overproduced in *E. coli* C43(DE3) (Lucigen). *E. coli* C43(DE3) cells transformed with the expression plasmid pNY1452 were grown at 30°C to an optical density at 600 nm (OD$_{600}$) of 0.7 to 0.8 in LB medium [Bacto Tryptone (10 g/liter), yeast extract (5 g/liter), and NaCl (10 g/liter); without pH adjustment] supplemented with ampicillin (50 µg/ml), followed by induction of overexpression with 0.1 mM IPTG and incubation at 30°C for an additional 4 hours. Cells were harvested by centrifugation and lysed by sonication in 10 mM tris-HCl (pH 7.4) with 150 mM NaCl. The cell lysates were centrifuged at 40,000*g* for 45 min at 4°C. Subsequently, the supernatant was separated by ultracentrifugation at 200,000*g* for 90 min at 4°C. The membrane fraction collected as precipitate was suspended in 10 mM tris-HCl (pH 7.4) with 150 mM NaCl and was ultracentrifuged again under the same conditions. Last, the precipitated membrane fraction was suspended in 10 mM tris-Cl (pH 7.4) with 150 mM NaCl, and the total protein was quantified using the bicinchoninic acid assay. The resuspended membrane fraction was diluted to adjust the protein concentration to 10 mg/ml using bovine serum albumin as a standard.

*Ec*RseP was solubilized by adding an equal volume of a solubilization buffer containing 40 mM tris-HCl (pH 8.5), 150 mM NaCl, and 2% sucrose monododecanoate (SM) to the suspension of the membrane fraction. After incubation at 4°C for 1 hour, the mixture was ultracentrifuged at 210,000*g* for 90 min. at 4°C. The supernatant was applied to NZ-1 antibody–conjugated Sepharose resin (anti–PA tag), and the unbound fraction was washed out with a buffer containing 10 mM tris-HCl (pH 8.5), 150 mM NaCl, and 0.05% SM. *Ec*RseP was eluted from the resin with a buffer containing 10 mM tris-HCl (pH 8.5), 150 mM NaCl, 0.05% SM, and PA14 peptide (0.1 mg/ml; EGGVAMPGAEDDVV). The C-terminal tag was cleaved off by adding TEV protease to the elution fraction, followed by incubation at 20°C overnight. The reaction mixture was then applied to a Superdex 200 10/300 GL SEC column (Cytiva). The peak fraction containing putative monomeric *Ec*RseP was collected and again applied to the same SEC column to remove oligomeric *Ec*RseP and aggregated TEV protease. After the second round of SEC, monodisperse *Ec*RseP sample was obtained with high purity (~95%).

To produce *Kk*RseP, the plasmid pNY1432 was transformed into *E. coli* C43(DE3) harboring pRARE2. For the native *Kk*RseP, *E. coli* cells were grown at 30°C to an OD_{600} of 0.6 to 0.7 in an LB medium supplemented with ampicillin (50 μg/ml) and chloramphenicol (34 μg/ml), followed by induction of overexpression with 0.1 mM IPTG and incubation at 16°C for an additional 18 hours. To produce the SeMet-substituted *Kk*RseP, *E. coli* cells were first cultured in an LB medium supplemented with ampicillin (50 μg/ml) and chloramphenicol (34 μg/ml) grown at 30°C overnight. The cells were further inoculated into M9 medium supplemented with ampicillin (50 μg/ml) and chloramphenicol (34 μg/ml) and grown at 30°C. At an OD_{600} of 0.3, a mixture of amino acids was added to the medium where the final concentrations were as follows: lysine (100 mg/ml), phenylalanine (100 mg/ml), threonine (100 mg/ml), valine (50 mg/ml), leucine (50 mg/ml), isoleucine (50 mg/ml), and SeMet (60 mg/ml). At an OD_{600} of 0.7 to 0.8, 0.1 mM IPTG was added to induce the overproduction, followed by incubation at 16°C overnight. Harvested cells were lysed by sonication in 10 mM tris-HCl (pH 7.4) with 150 mM NaCl, followed by centrifugation at 20,000*g* for 30 min at 4°C. Subsequently, the supernatant was further separated by ultracentrifugation at 200,000*g* for 60 min at 4°C. The collected membrane fraction was lastly suspended in 20 mM tris-HCl (pH 8.0), 300 mM NaCl, 15% glycerol, and 0.1 mM phenylmethylsulfonyl fluoride (PMSF), and the total protein concentration was adjusted to 10 mg/ml.

*Kk*RseP was solubilized by adding an equal volume of a solubilization buffer containing 40 mM tris-HCl (pH 8.0), 300 mM NaCl, 20 mM imidazole, 10% glycerol, 2% DDM, and 0.4% CHS to the suspension of the membrane fraction. After incubation at 4°C for 1 hour, the mixture was ultracentrifuged at 210,000*g* for 30 min at 4°C. The supernatant was applied to Ni-NTA agarose resin, and the unbound fraction was washed out with a buffer containing 20 mM tris-HCl (pH 8.0), 300 mM NaCl, 10% glycerol, 0.03% DDM, 0.006% CHS, and 50 mM imidazole. *Ec*RseP was eluted with a buffer containing 20 mM tris-HCl (pH 8.0), 300 mM NaCl, 10% glycerol, 0.03% DDM, 0.006% CHS, and 300 mM imidazole. The C-terminal tag was cleaved off by adding TEV protease to the elution fraction, followed by incubation at 20°C overnight. The reaction mixture was dialyzed against a buffer containing 20 mM tris-HCl (pH 8.0), 300 mM NaCl, 10% glycerol, 0.03% DDM, 0.006% CHS, and 10 mM imidazole and was applied to the Ni-NTA agarose resin, and the tag-cleaved *Kk*RseP was collected in the unbound fraction. *Kk*RseP was further purified with a Superdex 200 10/300 GL SEC column (Cytiva).

Crystallographic analysis of full-length RsePs

Batimastat (Toronto Research Chemicals) was added to the SEC elution fractions of *Ec*RseP and *Kk*RseP, respectively, at a final concentration of 300 μM. Subsequently, *Ec*RseP and *Kk*RseP were concentrated up to 7 to 12 mg/ml by ultrafiltration and incorporated into lipidic cubic phase (LCP) by mixing the protein solution and monoolein (NU-CHECK-PREP Inc.) with a volume ratio of 5:8 using two syringes attached with a coupler. Crystallization conditions were searched and optimized by microbatch crystallization method using Laminex sandwich plates and the MemMeso screening Kit (Molecular Dimensions). Aliquots (50 or 100 nl) of the protein-monoolein mixture were dispensed onto 96-well glass plates and overlaid with 800 nl of crystallization solution using a mosquito LCP (TTP LabTech) or Crystal Gryphon LCP (Art Robbins Instruments). The crystals of *Ec*RseP used for data collection were obtained in a

crystallization solution containing 30% (v/v) PEG 500 dimethyl ether, 100 mM NaCl, 100 mM $MgCl_2$, and 100 mM Hepes-Na (pH 7.0), while those of *Kk*RseP were generated from crystallization solutions containing 28 to 30% (v/v) PEG 500 monomethyl ether, 100 mM NaCl, 100 mM $CaCl_2$, and 100 mM Hepes-Na (pH 7.0). Crystals were harvested using MicroMounts (MiTeGen) or LithoLoops (Molecular Dimensions) and flash-frozen in liquid nitrogen.

Diffraction data from the crystals obtained from the LCP crystallization were collected at SPring-8 beamline BL32XU (*43*) using an EIGER X9M detector (Dectris). Microfocused x-rays with a beam size of 15 μm by 10 μm at wavelengths of 1.0000 Å (*Ec*RseP native data), 1.2800 Å (Zn-anomalous diffraction data), and 0.9700 Å (Se-anomalous diffraction data), respectively, were used for both raster scan and data collection. A dataset with a total oscillation range of 10° and 0.1° oscillations per frame was collected from each crystal under an absorbed dose of 10 megagrays. The partial datasets collected with the automated data collection system ZOO (*44*) were merged, integrated, and scaled using the KAMO system (*45*), which integrates BLEND (*46*), XDS, and XSCALE (*47, 48*). Diffraction intensities were converted to structure factors using the CCP4 suite where 5% of the unique reflections were randomly selected as a test set for the calculation of free *R* factor (*49*).

Initial phases of the SeMet-substituted *Kk*RseP crystal were determined by a combination of molecular replacement and single-wavelength anomalous diffraction methods (MR-SAD). After MR using the structure of *Kk*PDZ-C domain as a search model, the Se-SAD phasing was performed using phenix.autosol (*50*). The initial models were manually modified and fit into the electron density map using the program COOT (*51*). The updated models were refined with phenix.refine (*52*) iteratively while monitoring the stereochemistry with MolProbity (*53*). The structure of *Ec*RseP was solved by MR using the partial model of *Kk*RseP in addition to the individual *Ec*PDZ-N [Protein Data Bank (PDB) code: 2ZPL] and *Ec*PDZ-C (PDB code: 2ZPM) models (*29*). The PCT domain and TM4, where the conformations were largely different from those of *Kk*RseP, were modeled manually. Model modification, structure refinement, and validation were performed similarly to those for *Kk*RseP. Statistics for data collection and refinement are summarized in Table 1.

Structural superposition and RMSD calculation were performed by a pairwise alignment protocol using LSQKAB (*54*). Figures for protein structures were prepared with PyMOL (The PyMOL Molecular Graphics System, version 2.3, Schrödinger LLC).

Media for biochemical analysis

L medium [Bacto Tryptone (10 g/liter), yeast extract (5 g/liter), and NaCl (5 g/liter); pH adjusted to 7.2 by using NaOH] and M9 medium [without $CaCl_2$; (*55*)] supplemented with thiamine (2 μg/ml) and 0.4% glucose were used to culture *E. coli* cells. Ampicillin (50 μg/ml), chloramphenicol (20 μg/ml), and spectinomycin (50 μg/ml) were added for selecting transformants and for growing plasmid-harboring cells.

In vivo proteolytic activity assay of *Ec*RseP and *Kk*RseP and their derivatives

The in vivo proteolytic activities of *Ec*RseP and *Kk*RseP were analyzed essentially as described previously (*24, 56*). Precultured cells were inoculated into an M9 medium supplemented with 20 μg/ml of each of the 20 amino acids, thiamine (2 μg/ml), 0.4% glucose, 1 mM IPTG, and 1 mM adenosine 3′,5′-cyclic monophosphate (cAMP) and grown at 30°C for 3 hours. The proteins were precipitated by

trichloroacetic acid (TCA) treatment, washed with acetone, suspended in SDS sample buffer with 2-mercaptoethanol (2ME), and analyzed by Laemmli SDS-PAGE and immunoblotting using an Immobilon membrane filter (MilliporeSigma) and appropriate antibodies. Proteins were visualized by a Lumino image analyzer LAS-4000 mini (Cytiva) using ECL (enhanced chemiluminescence) or ECL Prime Western Blotting Detection Reagents (Cytiva). Rabbit polyclonal anti–hemagglutinin (HA) [HA-probe (Y-11), Santa Cruz Biotechnology], anti–maltose-binding protein (MBP) (57), anti-EcRseP (19), and anti-SecB (21) antibodies and rat monoclonal anti-PA antibodies (58) were used for immunoblotting. Also, for detection of His-tagged proteins, anti-His antibodies from the Penta-His HRP Conjugate Kit (Qiagen) were used. In the short induction method, precultured cells were inoculated into an L medium with 0.4% glucose and grown at 30°C for 2.5 hours. Collected cells were suspended in 100 μl of L medium and preincubated at 30°C for 10 min in an Eppendorf Thermomixer comfort (600 rpm). After the addition of 1 mM IPTG, the cells were incubated at 30°C for 15 min with shaking. Last, the proteins were precipitated by the TCA treatment described above. Cleavage efficiencies of the substrates were calculated according to the following equation: cleavage efficiency (%) = 100 × (cleaved)/[(cleaved) + (full length)], where (cleaved) and (full length) are intensities of the respective bands.

In vitro substrate cleavage assay with purified EcRseP or KkRseP
Model substrate HA-RseA148 was synthesized using the PUREfrex 1.0 reconstituted cell-free protein synthesis kit [Gene Frontier Co., Japan; (59, 60)], using a template DNA (PCR-amplified from pYH18) and standard reagents including 0.02% DDM and ^{35}S-labeled methionine (^{35}S-Met). EcRseP or KkRseP was purified according to the same procedures as those for the samples for crystallization. Synthesized ^{35}S-labeled substrate was mixed with purified EcRseP [final concentration, 2.5 ng/μl (50 nM)], KkRseP [final concentration, 100 ng/μl (2.0 μM)], or each of the respective protein buffers (mock) and incubated at 37°C in buffer containing 50 mM tris-HCl (pH 8.1), 2.5% glycerol, 5 μM zinc acetate, 0.05% DDM, 100 mM NaCl, 10 mM DTT, and 5 mM zinc chelator 1,10-phenanthroline (PT+) or 5% dimethyl sulfoxide (DMSO; PT−) with shaking in an Eppendorf Thermomixer comfort (500 rpm) for the indicated periods. Samples were then mixed with an equal volume of 2× SDS sample buffer plus 2ME and boiled for 5 min. The proteins were separated by SDS-PAGE using a 15% bis-tris gel and MES SDS running buffer (61) and visualized using a PhosphorImager BAS5000 (Cytiva).

In vivo batimastat sensitivity assay
Batimastat inhibition of in vivo proteolytic activity of RseP derivatives was evaluated using a mutant strain that lacks the acrA gene coding a component of a multidrug efflux pump to increase the sensitivity to batimastat as described previously (27) with several modifications. YH2902 (ΔrseA ΔrseP ΔacrA) cells harboring two plasmids encoding an EcRseP derivative (pYH825 based) and a model substrate HA-MBP-RseA(LY1)148 (pYH124) were inoculated into L medium with 0.4% glucose and grown at 30°C for 2.5 hours. Collected cells were suspended in L medium and divided into three portions. Each portion received 12.5, 3.125, or 0 μM (final concentration) batimastat (MilliporeSigma, the stock solution of batimastat was dissolved in DMSO) and preincubated at 30°C for 10 min in an Eppendorf Thermomixer comfort (600 rpm). Samples were mixed

with IPTG (final concentration, 1 mM) to induce protein expression and incubated for 1 hour with shaking. Proteins were TCA-precipitated and analyzed by SDS-PAGE and immunoblotting.

Substituted cysteine accessibility analysis of single-cysteine EcRseP or KkRseP mutants
A mal-PEG accessibility assay was performed with single-Cys mutants of EcRseP or KkRseP using essentially the same method as described previously (20, 56). KK374 cells (57) carrying a plasmid encoding a tagless EcRseP Cys mutant or a KkRseP Cys mutant with an internal PA14 tag were cultured in L medium containing 0.4% glucose, 1 mM IPTG, and 1 mM cAMP at 30°C for 2.5 hours and converted to spheroplasts by lysozyme/EDTA treatment as described previously (29). Spheroplast samples were treated with water or 2% Triton X-100 at 0°C for 3 min in the presence of 5 mM MgCl$_2$, 1 mM PMSF, and 1 mM tris(2-carboxyethyl)phosphine (TCEP; MilliporeSigma). Samples were mixed with an equal volume of 2× reaction buffer [60 mM tris-HCl (pH 8.1) and 2 mM mal-PEG (MilliporeSigma)] and incubated at 4°C for the indicated periods. The Cys modification reaction was stopped by adding 10% 2ME. The proteins were TCA-precipitated and analyzed by SDS-PAGE and immunoblotting.

Single-Cys EcRseP mutants were modified in two steps with AMS and mal-PEG using essentially the same method as described previously (21, 56). Spheroplast samples of KK374 cells expressing a single-Cys mutant of RseP-His$_6$-Myc (RseP-HM) were prepared as above and then treated with water or 1% Triton X-100 at 0°C for 30 min in the presence of 10 mM MgCl$_2$, 1 mM PMSF, and 1 mM TCEP. After prewarming at 24°C for 5 min, samples were treated with 1 mM AMS (Thermo Fisher Scientific) in the presence or absence of 1% Triton X-100 at 24°C for 5 min. Following quenching of AMS by incubation with 62.5 mM DTT at 24°C for 18 min, the proteins were precipitated and washed with 5% TCA. Samples were solubilized in 100 mM tris-HCl (pH 8.1) containing 1% SDS and 1 mM TCEP and treated with 5 mM mal-PEG at 37°C for 1 hour with vigorous shaking to modify free thiols. AMS/mal-PEG–modified proteins were analyzed by SDS-PAGE and immunoblotting. The proportion of RseP-HM Cys mutants modified with AMS was calculated according to the following equation: AMS modification (%) = 100 × (a − b)/a, in which a is the ratio of the mal-PEG–modified forms to total RseP-HM in the control sample that is prepared without AMS treatment, and b is the ratio of the mal-PEG–modified forms to total RseP-HM in the AMS-treated sample. For immunoblotting analysis of mal-PEG–labeled proteins, an Immobilon-P^{SQ} membrane filter (MilliporeSigma) and transfer buffer containing 24 mM tris-base, 192 mM glycine, 10% methanol, and 0.05% SDS were used.

Complementation assay
E. coli KK31 [ΔrseP/pKK6 (P$_{BAD}$-rseP)] cells harboring a plasmid encoding EcRseP or its derivatives under the lac promoter were grown at 30°C in an L medium containing 0.02% L-arabinose for 2 hours. The cultures were serially diluted with saline, and 3 μl of the diluted cultures was spotted on L agar plates containing 1 mM IPTG to test complementation or 0.02% L-arabinose as a control for monitoring total cell counts. The plates were incubated at 30°C for the indicated period.

β-Galactosidase activity assay
The σ^E activity was assayed by monitoring β-galactosidase (LacZ) activity expressed from a chromosomal σ^E-dependent lacZ reporter

SCIENCE ADVANCES | RESEARCH ARTICLE

gene (*rpoH*P3-*lacZ*). Cells were grown at 30°C for 5 hours in an L medium with 0.1 mM IPTG and 1 mM cAMP. The LacZ activity of growing cells was measured using essentially the same method as previously described (*21*).

Site-directed in vivo photocrosslinking

Site-directed in vivo photocrosslinking was carried out using essentially the same method as previously described (*21*). Cells harboring pEVOL-pBpF and a plasmid encoding an RseP(E23Q)-HM derivative were grown at 30°C for 4 hours in an M9 medium containing 0.5 mM *p*BPA (Bachem AG). After adding spectinomycin (100 µg/ml) to stop further protein synthesis, a portion of the culture was withdrawn and ultraviolet (UV)–irradiated for 10 min at 4°C using a B-100 AP UV lamp (365 nm; UVP LLC). Proteins were TCA-precipitated and dissolved in SDS sample buffer with 2ME.

Disulfide cross-linking–mediated domain immobilization experiment

The in vivo proteolytic activity of *Ec*RseP after domain tethering by disulfide cross-linking was examined as follows. AD2544 cells harboring two independently inducible plasmids, each encoding an RseP derivative with a pair of Cys mutations under the P_{lac} promoter (pYH835 based) or the model substrate HA-MBP-RseA(LY1)148 (pTM949) under the P_{BAD} promoter, were used. Precultured cells were inoculated into L medium with 0.4% glucose, grown at 30°C for 1.5 hours, and divided into two portions. Collected cells were washed with and resuspended in 150 µl of L medium with 5 mM IPTG and incubated at 30°C for 30 min in an Eppendorf Thermomixer comfort (600 rpm) to induce expression of the RseP derivatives. After incubation, each of the two samples was washed with IPTG-free L medium, resuspended in L medium with 5 mM diamide (for oxidation) or 10 mM DTT (for reduction), and further incubated at 30°C for 30 min. The cells were washed again with L medium and resuspended in L medium containing 0.02% L-arabinose with (for the +DTT sample) or without (for the +diamide sample) 1 mM TCEP and incubated at 30°C for 30 min to induce substrate expression. Last, proteins were precipitated with TCA, resuspended in SDS sample buffer without 2ME, and analyzed by SDS-PAGE and immunoblotting.

To evaluate the efficiency of intramolecular disulfide cross-linking for double-Cys RseP, all TCA-precipitated postreaction samples were dissolved in 100 mM tris-HCl (pH 8.1) with 1% SDS and vigorously shaken for 30 min at room temperature. Then, the samples were divided into two portions, treated with 0 or 1 mM mal-PEG at 37°C for 1 hour with vigorous shaking to modify free thiols, mixed with 2× SDS sample buffer containing 2ME, and lastly analyzed by SDS-PAGE and immunoblotting.

Multiple alignment analysis of bacterial RseP homologs

Selection and amino acid sequence alignment of RseP homologs were performed as follows. BLAST search (blastp) (https://blast.ncbi.nlm.nih.gov/Blast.cgi) was performed, using the amino acid sequence of *Kk*RseP [*K. koreensis* str. DSM 16069: Kkor_1905 (UniProtKB: C7R5Z1)] as the query, against the nonredundant UniProtKB/SwissProt sequence database. From the 66 S2P homologs found by this search, duplicates, nonbacterial homologs, and homologs with obviously different molecular sizes were manually excluded, leaving 39 bacterial homologs. Multiple sequence alignment was performed with these 39 species by the Clustal W ver.2.1 program (www.clustal.org/clustal2)

using the genetic information processing software Genetyx (GENETYX Corporation, Japan).

SUPPLEMENTARY MATERIALS

Supplementary material for this article is available at https://science.org/doi/10.1126/sciadv.abp9011

REFERENCES AND NOTES

1. M. S. Brown, J. Ye, R. B. Rawson, J. L. Goldstein, Regulated intramembrane proteolysis: A control mechanism conserved from bacteria to humans. *Cell* **100**, 391–398 (2000).
2. H. A. Beard, M. Barniol-Xicota, J. Yang, S. H. L. Verhelst, Discovery of cellular roles of intramembrane proteases. *ACS Chem. Biol.* **14**, 2372–2388 (2019).
3. N. Kühnle, V. Dederer, M. K. Lemberg, Intramembrane proteolysis at a glance: From signalling to protein degradation. *J. Cell Sci.* **132**, jcs217745 (2019).
4. N. Suzuki, T. T. Cheung, X. D. Cai, A. Odaka, L. Otvos Jr., C. Eckman, T. E. Golde, S. G. Younkin, An increased percentage of long amyloid β protein secreted by familial amyloid β protein precursor (βAPP₇₁₇) mutants. *Science* **264**, 1336–1340 (1994).
5. D. J. Selkoe, Alzheimer's disease: Genes, proteins, and therapy. *Physiol. Rev.* **81**, 741–766 (2001).
6. J. S. Schneider, M. S. Glickman, Function of site-2 proteases in bacteria and bacterial pathogens. *Biochim. Biophys. Acta* **1828**, 2808–2814 (2013).
7. S. Urban, Making the cut: Central roles of intramembrane proteolysis in pathogenic microorganisms. *Nat. Rev. Microbiol.* **7**, 411–423 (2009).
8. L. Sun, X. Li, Y. Shi, Structural biology of intramembrane proteases: Mechanistic insights from rhomboid and S2P to γ-secretase. *Curr. Opin. Struct. Biol.* **37**, 97–107 (2016).
9. M. S. Wolfe, Intramembrane proteolysis. *Chem. Rev.* **109**, 1599–1612 (2009).
10. R. B. Rawson, N. G. Zelenski, D. Nijhawan, J. Ye, J. Sakai, M. T. Hasan, T. Y. Chang, M. S. Brown, J. L. Goldstein, Complementation cloning of S2P, a gene encoding a putative metalloprotease required for intramembrane cleavage of SREBPs. *Mol. Cell* **1**, 47–57 (1997).
11. J. Sakai, E. A. Duncan, R. B. Rawson, X. Hua, M. S. Brown, J. L. Goldstein, Sterol-regulated release of SREBP-2 from cell membranes requires two sequential cleavages, one within a transmembrane segment. *Cell* **85**, 1037–1046 (1996).
12. R. B. Rawson, The site-2 protease. *Biochim. Biophys. Acta* **1828**, 2801–2807 (2013).
13. J. Ye, R. B. Rawson, R. Komuro, X. Chen, U. P. Davé, R. Prywes, M. S. Brown, J. L. Goldstein, ER stress induces cleavage of membrane-bound ATF6 by the same proteases that process SREBPs. *Mol. Cell* **6**, 1355–1364 (2000).
14. K. Kanehara, Y. Akiyama, K. Ito, Characterization of the *yaeL* gene product and its S2P-protease motifs in *Escherichia coli*. *Gene* **281**, 71–79 (2001).
15. L. N. Kinch, K. Ginalski, N. V. Grishin, Site-2 protease regulated intramembrane proteolysis: Sequence homologs suggest an ancient signaling cascade. *Protein Sci.* **15**, 84–93 (2006).
16. B. M. Alba, J. A. Leeds, C. Onufryk, C. Z. Lu, C. A. Gross, DegS and YaeL participate sequentially in the cleavage of RseA to activate the σ^E-dependent extracytoplasmic stress response. *Genes Dev.* **16**, 2156–2168 (2002).
17. K. Kanehara, K. Ito, Y. Akiyama, YaeL (EcfE) activates the σ^E pathway of stress response through a site-2 cleavage of anti-σ^E, RseA. *Genes Dev.* **16**, 2147–2155 (2002).
18. S. E. Ades, Regulation by destruction: Design of the σ^E envelope stress response. *Curr. Opin. Microbiol.* **11**, 535–540 (2008).
19. Y. Hizukuri, Y. Akiyama, PDZ domains of RseP are not essential for sequential cleavage of RseA or stress-induced σ^E activation in vivo. *Mol. Microbiol.* **86**, 1232–1245 (2012).
20. Y. Hizukuri, T. Oda, S. Tabata, K. Tamura-Kawakami, R. Oi, M. Sato, J. Takagi, Y. Akiyama, T. Nogi, A structure-based model of substrate discrimination by a noncanonical PDZ tandem in the intramembrane-cleaving protease RseP. *Structure* **22**, 326–336 (2014).
21. T. Miyake, Y. Hizukuri, Y. Akiyama, Involvement of a membrane-bound amphiphilic helix in substrate discrimination and binding by an *Escherichia coli* S2P peptidase RseP. *Front. Microbiol.* **11**, 607381 (2020).
22. J. Shen, R. Prywes, Dependence of site-2 protease cleavage of ATF6 on prior site-1 protease digestion is determined by the size of the luminal domain of ATF6. *J. Biol. Chem.* **279**, 43046–43051 (2004).
23. Y. Zhang, P. M. Luethy, R. Zhou, L. Kroos, Residues in conserved loops of intramembrane metalloprotease SpoIVFB interact with residues near the cleavage site in pro-σ^K. *J. Bacteriol.* **195**, 4936–4946 (2013).
24. K. Akiyama, S. Mizuno, Y. Hizukuri, H. Mori, T. Nogi, Y. Akiyama, Roles of the membrane-reentrant β-hairpin-like loop of RseP protease in selective substrate cleavage. *eLife* **4**, e08928 (2015).
25. K. Akiyama, Y. Hizukuri, Y. Akiyama, Involvement of a conserved GFG motif region in substrate binding by RseP, an *Escherichia coli* S2P protease. *Mol. Microbiol.* **104**, 737–751 (2017).
26. L. Feng, H. Yan, Z. Wu, N. Yan, Z. Wang, P. D. Jeffrey, Y. Shi, Structure of a site-2 protease family intramembrane metalloprotease. *Science* **318**, 1608–1612 (2007).

27. A. Konovalova, M. Grabowicz, C. J. Balibar, J. C. Malinverni, R. E. Painter, D. Riley, P. A. Mann, H. Wang, C. G. Garlisi, B. Sherborne, N. W. Rigel, D. P. Ricci, T. A. Black, T. Roemer, T. J. Silhavy, S. S. Walker, Inhibitor of intramembrane protease RseP blocks the σ^E response causing lethal accumulation of unfolded outer membrane proteins. *Proc. Natl. Acad. Sci. U.S.A.* **115**, E6614–E6621 (2018).

28. R. Tamura-Sakaguchi, R. Aruga, M. Hirose, T. Ekimoto, T. Miyake, Y. Hizukuri, R. Oi, M. K. Kaneko, Y. Kato, Y. Akiyama, M. Ikeguchi, K. Iwasaki, T. Nogi, Moving toward generalizable NZ-1 labeling for 3D structure determination with optimized epitope-tag insertion. *Acta Crystallogr. D Struct. Biol.* **77**, 645–662 (2021).

29. K. Inaba, M. Suzuki, K. I. Maegawa, S. Akiyama, K. Ito, Y. Akiyama, A pair of circularly permuted PDZ domains control RseP, the S2P family intramembrane protease of *Escherichia coli*. *J. Biol. Chem.* **283**, 35042–35052 (2008).

30. D. M. Bolduc, D. R. Montagna, Y. Gu, D. J. Selkoe, M. S. Wolfe, Nicastrin functions to sterically hinder γ-secretase-substrate interactions driven by substrate transmembrane domain. *Proc. Natl. Acad. Sci. U.S.A.* **113**, E509–E518 (2016).

31. S. Cho, R. P. Baker, M. Ji, S. Urban, Ten catalytic snapshots of rhomboid intramembrane proteolysis from gate opening to peptide release. *Nat. Struct. Mol. Biol.* **26**, 910–918 (2019).

32. Z. Wu, N. Yan, L. Feng, A. Oberstein, H. Yan, R. P. Baker, L. Gu, P. D. Jeffrey, S. Urban, Y. Shi, Structural analysis of a rhomboid family intramembrane protease reveals a gating mechanism for substrate entry. *Nat. Struct. Mol. Biol.* **13**, 1084–1091 (2006).

33. G. Yang, R. Zhou, Q. Zhou, X. Guo, C. Yan, M. Ke, J. Lei, Y. Shi, Structural basis of Notch recognition by human γ-secretase. *Nature* **565**, 192–197 (2019).

34. S. W. Dickey, R. P. Baker, S. Cho, S. Urban, Proteolysis inside the membrane is a rate-governed reaction not driven by substrate affinity. *Cell* **155**, 1270–1281 (2013).

35. K. Koide, K. Ito, Y. Akiyama, Substrate recognition and binding by RseP, an *Escherichia coli* intramembrane protease. *J. Biol. Chem.* **283**, 9562–9570 (2008).

36. S. Olenic, F. Buchanan, J. VanPortfliet, D. Parrell, L. Kroos, Conserved proline residues of *Bacillus subtilis* intramembrane metalloprotease SpoIVFB are important for substrate interaction and cleavage. *J. Bacteriol.* **204**, JB0038621 (2022).

37. S. Halder, D. Parrell, D. Whitten, M. Feig, L. Kroos, Interaction of intramembrane metalloprotease SpoIVFB with substrate Pro-σ^K. *Proc. Natl. Acad. Sci. U.S.A.* **114**, E10677–E10686 (2017).

38. D. Z. Rudner, P. Fawcett, R. Losick, A family of membrane-embedded metalloproteases involved in regulated proteolysis of membrane-associated transcription factors. *Proc. Natl. Acad. Sci. U.S.A.* **96**, 14765–14770 (1999).

39. R. Zhou, G. Yang, X. Guo, Q. Zhou, J. Lei, Y. Shi, Recognition of the amyloid precursor protein by human γ-secretase. *Science* **363**, eaaw0930 (2019).

40. S. Zoll, S. Stanchev, J. Began, J. Škerle, M. Lepšík, L. Peclinovská, P. Majer, K. Strisovsky, Substrate binding and specificity of rhomboid intramembrane protease revealed by substrate-peptide complex structures. *EMBO J.* **33**, 2408–2421 (2014).

41. Y. Fujii, M. Kaneko, M. Neyazaki, T. Nogi, Y. Kato, J. Takagi, PA tag: A versatile protein tagging system using a super high affinity antibody against a dodecapeptide derived from human podoplanin. *Protein Expr. Purif.* **95**, 240–247 (2014).

42. C. Han, J. Sikorski, A. Lapidus, M. Nolan, T. Glavina del Rio, H. Tice, J. F. Cheng, S. Lucas, F. Chen, A. Copeland, N. Ivanova, K. Mavromatis, G. Ovchinnikova, A. Pati, D. Bruce, L. Goodwin, S. Pitluck, A. Chen, K. Palaniappan, M. Land, L. Hauser, Y. J. Chang, C. D. Jeffries, P. Chain, E. Saunders, T. Brettin, M. Göker, B. J. Tindall, J. Bristow, J. A. Eisen, V. Markowitz, P. Hugenholtz, N. C. Kyrpides, H. P. Klenk, J. C. Detter, Complete genome sequence of *Kangiella koreensis* type strain (SW-125^T). *Stand Genomic Sci.* **1**, 226–233 (2009).

43. K. Hirata, Y. Kawano, G. Ueno, K. Hashimoto, H. Murakami, K. Hasegawa, T. Hikima, T. Kumasaka, M. Yamamoto, Achievement of protein micro-crystallography at SPring-8 beamline BL32XU. *J. Phys. Conf. Ser.* **425**, 012002 (2013).

44. K. Hirata, K. Yamashita, G. Ueno, Y. Kawano, K. Hasegawa, T. Kumasaka, M. Yamamoto, *ZOO*: An automatic data-collection system for high-throughput structure analysis in protein microcrystallography. *Acta Crystallogr. D Struct. Biol.* **75**, 138–150 (2019).

45. K. Yamashita, K. Hirata, M. Yamamoto, *KAMO*: Towards automated data processing for microcrystals. *Acta Crystallogr. D Struct. Biol.* **74**, 441–449 (2018).

46. J. Foadi, P. Aller, Y. Alguel, A. Cameron, D. Axford, R. L. Owen, W. Armour, D. G. Waterman, S. Iwata, G. Evans, Clustering procedures for the optimal selection of data sets from multiple crystals in macromolecular crystallography. *Acta Crystallogr. D Struct. Biol.* **69**, 1617–1632 (2013).

47. W. Kabsch, Automatic processing of rotation diffraction data from crystals of initially unknown symmetry and cell constants. *J. Appl. Cryst.* **26**, 795–800 (1993).

48. W. Kabsch, XDS. *Acta Crystallogr. D Biol. Crystallogr.* **66**, 125–132 (2010).

49. M. D. Winn, C. C. Ballard, K. D. Cowtan, E. J. Dodson, P. Emsley, P. R. Evans, R. M. Keegan, E. B. Krissinel, A. G. W. Leslie, A. McCoy, S. J. McNicholas, G. N. Murshudov, N. S. Pannu, E. A. Potterton, H. R. Powell, R. J. Read, A. Vagin, K. S. Wilson, Overview of the CCP4 suite and current developments. *Acta Crystallogr. D Biol. Crystallogr.* **67**, 235–242 (2011).

50. T. C. Terwilliger, P. D. Adams, R. J. Read, A. J. McCoy, N. W. Moriarty, R. W. Grosse-Kunstleve, P. V. Afonine, P. H. Zwart, L. W. Hung, Decision-making in structure solution using Bayesian estimates of map quality: The PHENIX AutoSol wizard. *Acta Crystallogr. D Biol. Crystallogr.* **65**, 582–601 (2009).

51. P. Emsley, B. Lohkamp, W. G. Scott, K. Cowtan, Features and development of *Coot*. *Acta Crystallogr. D Biol. Crystallogr.* **66**, 486–501 (2010).

52. P. V. Afonine, R. W. Grosse-Kunstleve, N. Echols, J. J. Headd, N. W. Moriarty, M. Mustyakimov, T. C. Terwilliger, A. Urzhumtsev, P. H. Zwart, P. D. Adams, Towards automated crystallographic structure refinement with *phenix.refine*. *Acta Crystallogr. D Biol. Crystallogr.* **68**, 352–367 (2012).

53. V. B. Chen, W. B. Arendall III, J. J. Headd, D. A. Keedy, R. M. Immormino, G. J. Kapral, L. W. Murray, J. S. Richardson, D. C. Richardson, *MolProbity*: All-atom structure validation for macromolecular crystallography. *Acta Crystallogr. D Biol. Crystallogr.* **66**, 12–21 (2010).

54. W. Kabsch, A solution for the best rotation to relate two sets of vectors. *Acta Crystallogr.* **32**, 922–923 (1976).

55. J. H. Miller, *Experiments in Molecular Genetics* (Cold Spring Harbor Laboratory Press, 1972).

56. Y. Hizukuri, K. Akiyama, Y. Akiyama, Biochemical characterization of function and structure of RseP, an *Escherichia coli* S2P protease. *Methods Enzymol.* **584**, 1–33 (2017).

57. Y. Akiyama, K. Kanehara, K. Ito, RseP (YaeL), an *Escherichia coli* RIP protease, cleaves transmembrane sequences. *EMBO J.* **23**, 4434–4442 (2004).

58. K. Yoshitani, Y. Hizukuri, Y. Akiyama, An *in vivo* protease activity assay for investigating the functions of the *Escherichia coli* membrane protease HtpX. *FEBS Lett.* **593**, 842–851 (2019).

59. Y. Shimizu, A. Inoue, Y. Tomari, T. Suzuki, T. Yokogawa, T. Nishikawa, T. Ueda, Cell-free translation reconstituted with purified components. *Nat. Biotechnol.* **19**, 751–755 (2001).

60. Y. Shimizu, T. Kanamori, T. Ueda, Protein synthesis by pure translation systems. *Methods* **36**, 299–304 (2005).

61. T. Yokoyama, T. Niinae, K. Tsumagari, K. Imami, Y. Ishihama, Y. Hizukuri, Y. Akiyama, The *Escherichia coli* S2P intramembrane protease RseP regulates ferric citrate uptake by cleaving the sigma factor regulator FecR. *J. Biol. Chem.* **296**, 100673 (2021).

62. K. Koide, S. Maegawa, K. Ito, Y. Akiyama, Environment of the active site region of RseP, an *Escherichia coli* regulated intramembrane proteolysis protease, assessed by site-directed cysteine alkylation. *J. Biol. Chem.* **282**, 4553–4560 (2007).

63. N. Sakaguchi, T. Kimura, S. Matsushita, S. Fujimura, J. Shibata, M. Araki, T. Sakamoto, C. Minoda, K. Kuwahara, Generation of high-affinity antibody against T cell-dependent antigen in the *Ganp* gene-transgenic mouse. *J. Immunol.* **174**, 4485–4494 (2005).

64. M. Kaneko, Y. Kato, H. Horiuchi, M. Osawa, Molecular characterization of a human monoclonal antibody to B antigen in ABO blood type. *Immunol. Lett.* **86**, 45–51 (2003).

65. M. K. Kaneko, A. Kunita, S. Abe, Y. Tsujimoto, M. Fukayama, K. Goto, Y. Sawa, Y. Nishioka, Y. Kato, Chimeric anti-podoplanin antibody suppresses tumor metastasis through neutralization and antibody-dependent cellular cytotoxicity. *Cancer Sci.* **103**, 1913–1919 (2012).

66. P. R. Evans, G. N. Murshudov, How good are my data and what is the resolution? *Acta Crystallogr. D Biol. Crystallogr.* **69**, 1204–1214 (2013).

67. A. Vagin, A. Teplyakov, MOLREP: An automated program for molecular replacement. *J. Appl. Cryst.* **30**, 1022–1025 (1997).

68. S. Q. Zheng, E. Palovcak, J. P. Armache, K. A. Verba, Y. Cheng, D. A. Agard, MotionCor2: Anisotropic correction of beam-induced motion for improved cryo-electron microscopy. *Nat. Methods* **14**, 331–332 (2017).

69. K. Zhang, Gctf: Real-time CTF determination and correction. *J. Struct. Biol.* **193**, 1–12 (2016).

70. A. Rohou, N. Grigorieff, CTFFIND4: Fast and accurate defocus estimation from electron micrographs. *J. Struct. Biol.* **192**, 216–221 (2015).

71. J. Zivanov, T. Nakane, B. O. Forsberg, D. Kimanius, W. J. Hagen, E. Lindahl, S. H. Scheres, New tools for automated high-resolution cryo-EM structure determination in RELION-3. *eLife* **7**, e42166 (2018).

72. E. F. Pettersen, T. D. Goddard, C. C. Huang, G. S. Couch, D. M. Greenblatt, E. C. Meng, T. E. Ferrin, UCSF Chimera—A visualization system for exploratory research and analysis. *J. Comput. Chem.* **25**, 1605–1612 (2004).

73. T. Baba, T. Ara, M. Hasegawa, Y. Takai, Y. Okumura, M. Baba, K. A. Datsenko, M. Tomita, B. L. Wanner, H. Mori, Construction of *Escherichia coli* K-12 in-frame, single-gene knockout mutants: The Keio collection. *Mol. Syst. Biol.* **2**, 2006.0008 (2006).

74. K. A. Datsenko, B. L. Wanner, One-step inactivation of chromosomal genes in *Escherichia coli* K-12 using PCR products. *Proc. Natl. Acad. Sci. U.S.A.* **97**, 6640–6645 (2000).

75. A. Kihara, Y. Akiyama, K. Ito, FtsH is required for proteolytic elimination of uncomplexed forms of SecY, an essential protein translocase subunit. *Proc. Natl. Acad. Sci. U.S.A.* **92**, 4532–4536 (1995).

76. T. J. Silhavy, M. L. Berman, L. W. Enquist, *Experiments with Gene Fusions* (Cold Spring Harbor Laboratory Press, 1984).

77. Y. Akiyama, T. Ogura, K. Ito, Involvement of FtsH in protein assembly into and through the membrane. I. Mutations that reduce retention efficiency of a cytoplasmic reporter. *J. Biol. Chem.* **269**, 5218–5224 (1994).

78. M. J. Casadaban, S. N. Cohen, Analysis of gene control signals by DNA fusion and cloning in *Escherichia coli*. *J. Mol. Biol.* **138**, 179–207 (1980).

79. J. Mecsas, P. E. Rouviere, J. W. Erickson, T. J. Donohue, C. A. Gross, The activity of σ^E, an *Escherichia coli* heat-inducible σ-factor, is modulated by expression of outer membrane proteins. *Genes Dev.* **7**, 2618–2628 (1993).

80. L. M. Guzman, D. Belin, M. J. Carson, J. Beckwith, Tight regulation, modulation, and high-level expression by vectors containing the arabinose P_{BAD} promoter. *J. Bacteriol.* **177**, 4121–4130 (1995).

81. K. Kanehara, K. Ito, Y. Akiyama, YaeL proteolysis of RseA is controlled by the PDZ domain of YaeL and a Gln-rich region of RseA. *EMBO J.* **22**, 6389–6398 (2003).

82. T. S. Young, I. Ahmad, J. A. Yin, P. G. Schultz, An enhanced system for unnatural amino acid mutagenesis in *E. coli*. *J. Mol. Biol.* **395**, 361–374 (2010).

83. P. P. Cherepanov, W. Wackernagel, Gene disruption in *Escherichia coli*: Tc[R] and Km[R] cassettes with the option of Flp-catalyzed excision of the antibiotic-resistance determinant. *Gene* **158**, 9–14 (1995).

84. M. Sakoh, K. Ito, Y. Akiyama, Proteolytic activity of HtpX, a membrane-bound and stress-controlled protease from *Escherichia coli*. *J. Biol. Chem.* **280**, 33305–33310 (2005).

Science Advances

Mechanistic insights into intramembrane proteolysis by E. coli site-2 protease homolog RseP

Yuki ImaizumiKazunori TakanukiTakuya MiyakeMizuki TakemotoKunio HirataMika HiroseRika OiTatsuya KobayashiKenichi MiyoshiRie ArugaTatsuhiko YokoyamaShizuka KatagiriHiroaki MatsuuraKenji IwasakiTakayuki KatoMika K. KanekoYukinari KatoMichiko TajiriSatoko AkashiOsamu NurekiYohei HizukuriYoshinori AkiyamaTerukazu Nogi

View the article online
https://www.science.org/doi/10.1126/sciadv.abp9011
Permissions
https://www.science.org/help/reprints-and-permissions